IEEE Transactions on Aerospace and Electronic Systems, Available online 17 August 2022
DOI:10.1109/TAES.2022.3199705

Three-Dimensional Biased Proportional Navigation Guidance Based on Spatial Rotation of Predicted Final Velocity

Namhoon Cho, Seokwon Lee, Hyo-Sang Shin, and Tae-Hun Kim

Abstract

This study presents the design of three-dimensional biased proportional navigation guidance laws for arrival at a stationary target along a desired direction based on spatial rotation of predicted final velocity vector. The focus is on full constructive derivation using vector-form expressions without introducing local representation of rotation such as Euler angles or quaternions. The proposed approach synthesises the bias command in the form of an angular velocity vector through realisation of the predictive control design philosophy, the direction which has been unexplored in a three-dimensional setting. The proposed approach avoids heuristic choices and approximations in the design process and hence overcomes the limitation of earlier studies. The vector-form design approach provides theoretical and practical advantages including rigour in derivation, clear geometric understandings about the problem provided by identification of the most effective direction for rotation of final velocity, independence from selection of a fixed coordinate system, avoidance of singularities in local representations, more direct trajectory shaping, and simple implementation.

Index Terms

Three-Dimensional, Biased Proportional Navigation Guidance, Predictive Correction, Final Velocity Direction, Vector Rotation

Nomenclature

$\mathbf{a}$	acceleration
$\mathbf{a}^{v\perp}$	lateral (normal) acceleration, perpendicular to vehicle velocity
e	predicted final velocity direction error, value in $[0, \pi]$ radians

Namhoon Cho, Seokwon Lee, and Hyo-Sang Shin are with the Centre for Autonomous and Cyber-Physical Systems, School of Aerospace, Transport and Manufacturing, Cranfield University, Cranfield, MK43 0AL, Bedfordshire, United Kingdom. e-mail: {n.cho, seokwon.lee, h.shin}@cranfield.ac.uk

Tae-Hun Kim is with the School of Mechanical and Aerospace Engineering, Sunchon National University, Suncheon, 57922, Republic of Korea. e-mail: tehunida@gmail.com

$\hat{\mathbf{k}}$	unit normal vector of manoeuvre plane
N	proportional navigation constant
r	distance between vehicle and target, i.e., range
$\mathbf{r}$	line-of-sight from vehicle to target
$\hat{\mathbf{r}}$	unit vector in the direction of line-of-sight
$\mathbf{v}$	vehicle velocity
$\hat{\mathbf{v}}$	unit vector in the direction of vehicle velocity
$\hat{\mathbf{v}}_{f_d}$	unit vector in the direction of desired final vehicle velocity
$\hat{\mathbf{v}}_{f_{pred}}$	unit vector in the direction of predicted final vehicle velocity
σ	three-dimensional lead angle, value in $[0, \pi]$ radians
ω_{bias}	bias angular velocity command
ω_f	angular velocity of predicted final vehicle velocity
ω_{f_d}	desired angular velocity of predicted final vehicle velocity
$\omega_r^{r\perp}$	angular velocity of line-of-sight, perpendicular to line-of-sight
ω_v	angular velocity of vehicle velocity
	Vector Notations
$\hat{(\cdot)}$	unit vector
$\dot{(\cdot)}$	derivative with respect to time
$(\cdot)'$	derivative with respect to range

I. Introduction

The capability to arrive at a point with a specific direction at the final time is an essential prerequisite for autonomous flying vehicles to accomplish missions by passing through a series of waypoints or a real target. Typical anti-ground and anti-ship missiles perform manoeuvres to achieve certain incidence direction in vertical and horizontal plane, respectively, at the end of midcourse phase to shape their trajectories as needed for enhanced survivability as well as increased attack effectiveness. However, the approximation of planar motion and corresponding manoeuvre strategy based on stitching two-dimensional movements are invalid in certain applications. The necessity of three-dimensional arrival direction control arises specifically from anti-air missiles that require certain angle of approach to establish a desirable collision geometry for enhancing seeker measurement quality or maximising final speed for higher manoeuvrability. Advanced anti-ground or anti-ship missile concepts involving in-flight target selection/update also require a guidance method that can effectively handle the changes in both manoeuvre plane and desired impact direction. Furthermore, three-dimensional guidance methods capable

of arrival direction control can be utilised as the near-optimal local planners inside sampling-based motion planning algorithms for safe and efficient movement of flying robots in obstacle-rich environment [1], [2]. Planetary landers that perform landing-site selection during the descent phase may also find a simple three-dimensional steering law useful to achieve a specific approach angle.

Three-dimensional guidance problems are in general much more challenging than their planar counterparts due to the complexities in mathematical formulation. Increased number of variables as well as additional degrees-of-freedom associated with the kinematic relations is one apparent cause. Non-uniqueness of the ways to define error variables quantifying the separation between performance outputs and their reference values is also a reason. Another significant difficulty in most endo-atmospheric problems is the constraint that the acceleration command should be perpendicular to the vehicle velocity to avoid demanding speed change which might easily be infeasible for aerodynamically-controlled vehicles. This restriction leads to a command structure for the under-actuated kinematic model representing acceleration command as the cross product of a vector with the vehicle velocity as discussed in [3], [4], thus the name *cross product steering*. Unlike the explicit guidance methods such as those developed in [5]–[7] based on a fully-actuated kinematic model performing *arbitrary steering* which permits the presence of tangential acceleration command, a cross product steering method can hardly be designed by using simple double integrator kinematics since propagation of its acceleration command given by a bilinear map is not easy. The aforementioned complexities of three-dimensional guidance with cross-product steering can commonly be observed in the studies on target interception [4], [8]–[17], target interception with evasive manoeuvre [18], target interception with impact direction constraint [19]–[24], path-following [25], [26], and leader-follower formation flight [27].

Target interception with a three-dimensional terminal direction constraint has been addressed by applying various control-theoretic approaches. A motivation to develop methods addressing the three-dimensional nature of the problem directly is to overcome the drawbacks of employing planar impact-angle-control guidance laws applied separately in two orthogonal planes. In the context of this study, previous studies can be categorised into two groups depending on the type of differential relations considered for development: i) multiple scalar equations, and ii) vector form equations. The methods in [28]–[38] were developed based on multiple scalar equations describing the motion of vehicle and line-of-sight with respect to a fixed coordinate system in $\mathbb{R}^3$. Although the formulation takes into account all the coupling effects in three-dimensional engagement kinematics, the system of equations may become ill-defined due to the inherent singularities of Euler angles used to describe directional quantities. Manipulation of many scalar equations may also hinder clear physical understanding of the closed-loop system. On the other hand, vector form equations are used with 1) the arbitrary steering form on two separate orthogonal planes

in [39], [40], 2) the arbitrary steering form for spatial motion in [6], [7], [41], [42], and 3) the cross product steering form in [19]–[24]. The methods employing vector formulation are in general simpler to understand and implement, while the optimisation-based techniques employing multiple scalar equations allows more flexibility.

Despite extensive efforts, a completely constructive approach to the design of Biased Proportional Navigation Guidance law (BPNG) according to the predictive control philosophy has not been addressed in three-dimensional space. As it was recognised well in [21], a single well-defined equation for guidance policy posed in three-dimensional space is desirable for practice. Only a few recent studies attempted to design three-dimensional algorithms in the form of BPNG [19]–[24] which belongs to the general family of cross product steering methods. However, the approaches taken in those studies to derive the command formula are quite empirical in the sense that they substantially rely on heuristic choices based on physical intuition and extension of previous knowledge about two-dimensional BPNG. Selection of the manoeuvre plane for three-dimensional engagement was highlighted in [19] in the context of midcourse guidance, but it resorted to simulation tests comparing different candidates rather than a deductive reasoning. The issue was left as an ambiguity of design process. The multi-stage strategy of [20] is essentially a planar technique as it separates alignment of the manoeuvre plane to the desired one before proceeding to in-plane control of impact angle. Also, the quaternion-based analysis presented in [22] regarding optimality and trajectory shaping is unnecessarily complicated. Most importantly, the design principle of predictive correction is not thoroughly realised in those earlier studies, leading to the limitation in showing the extensibility of the design process as a systematic framework to incorporate various trajectory shaping necessities. Unlike the studies on planar BPNGs such as [43]–[45], the notion of defining a performance output error as a difference between the instantaneous prediction of the final value and the desired value is not perceived in [21], [22] where the spatial BPNGs are developed to align the *current* velocity or line-of-sight with the desired terminal direction. That is, the prediction-centric perspective towards BPNG remains unexplored in a three-dimensional setup. A notable exception is [24] where the three-dimensional guidance law was derived to control the impact direction with respect to a manoeuvring target based on nullifying the error angle associated with the predicted terminal velocity direction. The method was obtained by employing a vector-form BPNG in the relative reference frame to define the three-dimensional relative motion of missile with respect to target. However, the notion of vector spatial rotation and the additional rotational degree-of-freedom around the final velocity direction have not been fully appreciated. In these regards, the study of three-dimensional BPNG is still incomplete.

This study primarily aims to develop a constructive framework of three-dimensional BPNGs for arrival direction control capable of additional trajectory shaping. The main novelty is a straightforward realisation

of the predictive control philosophy through spatial rotation of the *predicted* final velocity for the baseline Pure Proportional Navigation Guidance law (PPNG) onto the desired direction. Accordingly, the proposition is to design the angular velocity of the predicted velocity direction vector as the command to nullify the angular difference. This approach brings advantages in three-dimensional problems as it does not necessarily rely on a ground-fixed coordinate system. In addition, the design directly with vector form manipulation could be more elegant and clearer than the approach of considering approximate kinematic equations decoupled for motion in vertical and horizontal planes.

The proposed approach complements the limitations of relevant studies through novel vector-form formulation. To the best of our knowledge, this study introduces predictive spatial rotation of the final velocity for the first time as the design principle for three-dimensional BPNGs, without introducing local parametrisation that might be ill-defined such as Euler angle or quaternion. Understanding the action of bias command as the angular velocity of the predicted final velocity provides not only a solid theoretical foundation but also practical benefits. This point of view facilitates the analysis of optimality and final velocity direction error convergence. In particular, this study does not assume any small angle assumption for linearisation in the design and analysis. Another important contribution is that the rotation of predicted final velocity around the axis of desired final direction, which is decoupled from regulation of the final direction error, provides one additional degree-of-freedom in the design of bias command vector to meet further trajectory shaping objectives. For example, the additional rotation enables three-dimensional impact direction control combined with weaving manoeuvre pattern for evasion or target observability enhancement. Most of all, the proposed three-dimensional BPNG is simple to implement and flexible enough to achieve a wide range of arrival directions. A Julia implementation of the proposed BPNG is accessible via [46].

The rest of the paper is organised as follows: Section II summarises the preliminary mathematical knowledge about vector products and rotation. Section III first derives the expressions for predicted final velocity and its time-derivate in vector form. The latter part of Sec. III presents the proposed methodology to design a bias command for control of arrival direction based on three-dimensional rotation of predicted final velocity. Section III also discusses possible extensions to incorporate additional trajectory shaping goals and modifications to keep the lead angle below a limit. In Sec. IV, numerical simulation examples validate the proposed BPNG design principle and demonstrate the closed-loop trajectory characteristics. Section V provides concluding remarks.

II. Preliminaries

This section briefly presents some of the basic facts related to algebraic manipulation of three-dimensional vectors that will be frequently recalled throughout the paper. Lemma 1 provides a summary of useful relations for triple products, Lemma 2 explains the Rodrigues' rotation formula, and Lemma 3 describes the time-derivative of unit vector and the associated angular velocity.

A. Triple Product

Lemma 1 (Triple Product Rules)**.**

$$\mathbf{a} \cdot (\mathbf{b} \times \mathbf{c}) = \mathbf{b} \cdot (\mathbf{c} \times \mathbf{a}) = \mathbf{c} \cdot (\mathbf{a} \times \mathbf{b}) \tag{1}$$

$$(\mathbf{a} \cdot (\mathbf{b} \times \mathbf{c}))\, \mathbf{a} = (\mathbf{a} \times \mathbf{b}) \times (\mathbf{a} \times \mathbf{c}) \tag{2}$$

$$\mathbf{a} \times (\mathbf{b} \times \mathbf{c}) = (\mathbf{a} \cdot \mathbf{c})\, \mathbf{b} - (\mathbf{a} \cdot \mathbf{b})\, \mathbf{c} \tag{3}$$

$$(\mathbf{a} \times \mathbf{b}) \times \mathbf{c} = \mathbf{a} \times (\mathbf{b} \times \mathbf{c}) - \mathbf{b} \times (\mathbf{a} \times \mathbf{c}) \tag{4}$$

$$\mathbf{a} \times (\mathbf{b} \times \mathbf{c}) + \mathbf{b} \times (\mathbf{c} \times \mathbf{a}) + \mathbf{c} \times (\mathbf{a} \times \mathbf{b}) = \mathbf{0} \tag{5}$$

B. Three-Dimensional Rotation of Vector

Rodrigues' rotation formula is a simple expression for the operation rotating a vector in three-dimensional space, given a rotation axis and angle.

Lemma 2 (Rodrigues' Rotation Formula)**.**
If $\mathbf{v}$ *is a vector in* $\mathbb{R}^3$ *and* $\mathbf{k}$ *is a unit vector describing an axis of rotation about which* $\mathbf{v}$ *rotates by an angle* θ *according to the right-hand rule, the Rodrigues' formula for the rotated vector* $\mathbf{v}_{rot}$ *is*

$$\mathbf{v}_{rot} = \mathbf{v} \cos\theta + (\mathbf{k} \times \mathbf{v}) \sin\theta + \mathbf{k}\, (\mathbf{k} \cdot \mathbf{v})\, (1 - \cos\theta) \tag{6}$$

Proof. See [47]–[49]. □

C. Angular Velocity of Unit Vector Induced by Time-Derivative

Lemma 3 (Time-Derivative and Angular Velocity of Unit Vector)**.**
The time-derivative of a three-dimensional unit vector $\mathbf{u}$ *can always be represented as*

$$\dot{\hat{\mathbf{u}}} = \boldsymbol{\omega}_u \times \hat{\mathbf{u}} \tag{7}$$

with an angular velocity $\boldsymbol{\omega}_u$*. The component of* $\boldsymbol{\omega}_u$ *perpendicular to the associated unit vector* $\hat{\mathbf{u}}$ *can be written as*

$$\boldsymbol{\omega}_u^{u\perp} = \hat{\mathbf{u}} \times \dot{\hat{\mathbf{u}}} \tag{8}$$

Also, Eq. (7) can be rewritten considering Eq. (8) as

$$\dot{\hat{\mathbf{u}}} = \boldsymbol{\omega}_u^{u\perp} \times \hat{\mathbf{u}} \tag{9}$$

Proof. See Appendices of [27]. □

III. Design of Command Vector

A. Problem Formulation and Kinematics

Consider the three-dimensional motion of a point mass vehicle M for which Fig. 1 shows the problem geometry both in three-dimensional and two-dimensional perspectives. The target T in Fig. 1 is a fixed

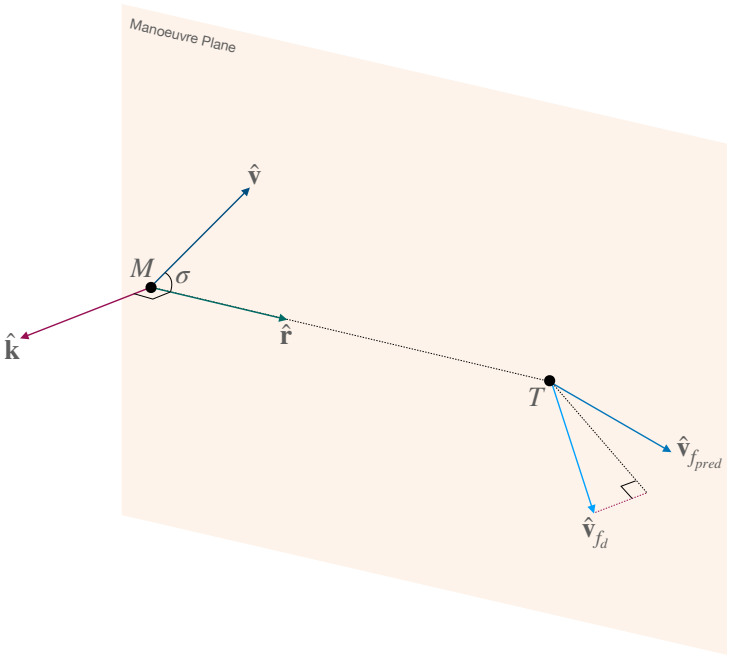

(a) Three-Dimensional View

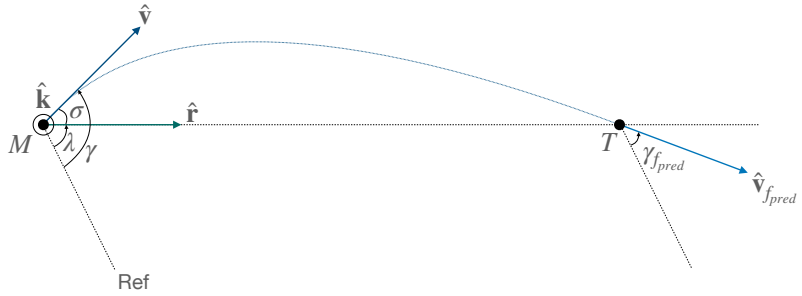

(b) Two-Dimensional View and Definition of Variables in Manoeuvre Plane

Fig. 1: Problem Geometry

point in space. Let $\mathbf{r}$ and $\mathbf{v}$ denote the Line-Of-Sight (LOS) from vehicle to target and vehicle velocity, respectively. The hat notation indicates that the quantity is a unit vector. Here, $\hat{\mathbf{r}} \triangleq \frac{\mathbf{r}}{\|\mathbf{r}\|}$ and $\hat{\mathbf{v}} \triangleq \frac{\mathbf{v}}{\|\mathbf{v}\|}$ denote the unit vectors in the direction of $\mathbf{r}$ and $\mathbf{v}$, respectively. Another unit vector $\hat{\mathbf{k}}$ is defined to be perpendicular to the instantaneous manoeuvre plane spanned by $\hat{\mathbf{r}}$ and $\hat{\mathbf{v}}$, i.e.,

$$\hat{\mathbf{k}} \triangleq \frac{\mathbf{r} \times \mathbf{v}}{\|\mathbf{r} \times \mathbf{v}\|} \tag{10}$$

Note that the instantaneous manoeuvre plane can rotate in three-dimensional space, that is, $\hat{\mathbf{k}}$ is not necessarily a fixed unit vector. In Fig. 1a, $\hat{\mathbf{v}}_{f_d}$ is the desired final velocity direction and $\hat{\mathbf{v}}_{f_{pred}}$ is the final velocity direction predicted at each instance as a result of motion governed by a baseline guidance law.

Figure 1b depicts the geometry and definitions of associated variables in the instantaneous manoeuvre plane. The angular separation between $\hat{\mathbf{r}}$ and $\hat{\mathbf{v}}$ along the manoeuvre plane is the three-dimensional lead angle defined as $\sigma \triangleq \cos^{-1}(\hat{\mathbf{r}} \cdot \hat{\mathbf{v}}) \in [0, \pi]$. By definition, we have $\cos\sigma = \hat{\mathbf{r}} \cdot \hat{\mathbf{v}}$ and $\sin\sigma = \|\hat{\mathbf{r}} \times \hat{\mathbf{v}}\|$. For the simplicity of explanation, we can consider a reference line on the manoeuvre plane as shown in Fig. 1b to define the flight path angle γ and the LOS angle λ as the amount of rotation from the reference line which is positive around the axis $\hat{\mathbf{k}}$ with the right-hand rule. The reference line is taken in a direction that render both γ and λ positive so that $\sigma = \gamma - \lambda$ holds. In accordance with the definition of γ, the predicted final flight path angle that corresponds to $\hat{\mathbf{v}}_{f_{pred}}$ is denoted by $\gamma_{f_{pred}}$.

According to Lemma 3, the time-derivative of LOS direction vector can be written as

$$\dot{\hat{\mathbf{r}}} = \boldsymbol{\omega}_r^{r\perp} \times \hat{\mathbf{r}} \tag{11}$$

where $\boldsymbol{\omega}_r^{r\perp}$ is the angular velocity of LOS given by

$$\boldsymbol{\omega}_r^{r\perp} = \frac{\mathbf{v} \times \mathbf{r}}{\|\mathbf{r}\|^2} = -\frac{v \sin\sigma}{r}\hat{\mathbf{k}} \tag{12}$$

where $v \triangleq \|\mathbf{v}\|$. Equation (12) shows that $\boldsymbol{\omega}_r^{r\perp}$ has no component in the redundant direction of $\hat{\mathbf{r}}$ since it is parallel to $\hat{\mathbf{k}}$. Also, the time-derivative of the range $r \triangleq \|\mathbf{r}\|$ can be expressed as

$$\dot{r} = -\mathbf{v} \cdot \hat{\mathbf{r}} = -v\cos\sigma \tag{13}$$

B. Predicted Final Velocity Direction Vector

Suppose that the vehicle employs a baseline guidance law for arrival at a stationary target. The present study takes the PPNG with a constant gain N given by

$$\mathbf{a}_{PPNG}^{v\perp} = N\boldsymbol{\omega}_r^{r\perp} \times \mathbf{v} \tag{14}$$

as the baseline that generates command for the normal acceleration. For a vehicle motion governed by the PPNG, it is well-known that the trajectory evolves on a manoeuvre plane which does not rotate through

the flight when the target is stationary. That is, the relative motion of a vehicle with respect to a target is a planar motion. Hence, the usual two-dimensional analytical results of PPNG applies well on this plane. With the angular quantities defined previously, the angular velocity of LOS can be written as

$$\boldsymbol{\omega}_r^{r\perp} = \dot{\lambda}\hat{\mathbf{k}} \tag{15}$$

Also, the normal acceleration of vehicle for the motion confined on a manoeuvre plane can be represented as

$$\mathbf{a}^{v\perp} = \dot{\gamma}\hat{\mathbf{k}} \times \mathbf{v} \tag{16}$$

By applying the PPNG given by Eq. (14) and assuming that the vehicle response to the commanded acceleration is lag-free, equating Eq. (16) and (14) yields

$$\dot{\gamma} = N\dot{\lambda} = \frac{N}{N-1}\dot{\sigma} \tag{17}$$

where the last equation is the result from the relation $\sigma = \gamma - \lambda$. Integrating Eq. (17) from t to t_f side by side gives the predicted final flight path angle as

$$\gamma_{f_{pred}} = \gamma - \frac{N}{N-1}\sigma = \lambda - \frac{1}{N-1}\sigma \tag{18}$$

since the PPNG terminates flight with zero final lead angle, i.e., $\sigma_{f_{pred}} = 0$. This shows that the predicted final velocity direction $\hat{\mathbf{v}}_{f_{pred}}$ is the unit vector obtained from rotating $\hat{\mathbf{v}}$ by an angle $\frac{N}{N-1}\sigma$, or equivalently, rotating $\hat{\mathbf{r}}$ by $\frac{1}{N-1}\sigma$, about the axis $-\hat{\mathbf{k}}$ according to the right-hand rule. Therefore, $\hat{\mathbf{v}}_{f_{pred}}$ can be expressed by using Lemma 2 as

$$\begin{aligned}\hat{\mathbf{v}}_{f_{pred}} &= \hat{\mathbf{v}}\cos\left(\frac{N}{N-1}\sigma\right) - \left(\hat{\mathbf{k}}\times\hat{\mathbf{v}}\right)\sin\left(\frac{N}{N-1}\sigma\right)\\ &= \hat{\mathbf{r}}\cos\left(\frac{1}{N-1}\sigma\right) - \left(\hat{\mathbf{k}}\times\hat{\mathbf{r}}\right)\sin\left(\frac{1}{N-1}\sigma\right)\end{aligned} \tag{19}$$

C. Rotation of Predicted Final Velocity Direction Vector and Error Dynamics

It is now well-known that a guidance law for satisfying given constraints such as impact angle or impact time conditions in addition to interception can be designed by taking the philosophy of predictive control approach in which an additive correction input besides the baseline input for the current time is designed. This allows the transfer of a predicted final value of an associated variable to its desired value [50]. The same principle applies in an identical manner to the design of a guidance law for three-dimensional flight with an extended set of equations representing the error dynamics. The main point of this study is that derivation of the equations directly in vector-form yields a design approach that is more elegant.

According to Lemma 3, the time-derivative of the unit vector in the direction of vehicle velocity should be represented in the following form

$$\dot{\hat{\mathbf{v}}} = \boldsymbol{\omega}_v \times \hat{\mathbf{v}} \tag{20}$$

Considering the definition of normal acceleration $\mathbf{a}^{v\perp} = \hat{\mathbf{v}} \times (\dot{\mathbf{v}} \times \hat{\mathbf{v}}) = v\dot{\hat{\mathbf{v}}}$ in conjunction with Eq. (20), a Biased Proportional Navigation Guidance law (BPNG) of the form $\mathbf{a}^{v\perp}_{BPNG} = \mathbf{a}^{v\perp}_{PPNG} + \mathbf{a}^{v\perp}_{bias}$ can be described equivalently in terms of the angular velocity command for the vehicle velocity as

$$\boldsymbol{\omega}_v = N\boldsymbol{\omega}_r^{r\perp} + \boldsymbol{\omega}_{bias} \tag{21}$$

Therefore, the bias angular velocity command $\boldsymbol{\omega}_{bias}$ is the input variable for three-dimensional guidance problem. One may easily verify by substituting Eq. (21) back in Eq. (20) and then multiplying v that the corresponding normal acceleration command is indeed

$$\mathbf{a}^{v\perp}_{BPNG} = \left(N\boldsymbol{\omega}_r^{r\perp} + \boldsymbol{\omega}_{bias}\right) \times \mathbf{v} \tag{22}$$

Figure 2 shows the definition of the error e associated with the problem of arrival at a target point along the desired final incidence direction. We can state that the objective is to design the magnitude and direction of $\boldsymbol{\omega}_{bias}$ to nullify the error e so that the vehicle arrives at the target with the desired final velocity direction.

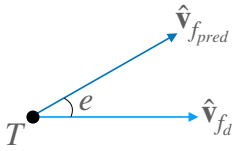

Fig. 2: Predicted Final Velocity Direction Error

The equation for the time-derivative of $\hat{\mathbf{v}}_{f_{pred}}$ is necessary to describe its evolution over time depending on the control input $\boldsymbol{\omega}_{bias}$. According to Lemma 3, it is obvious that the time-derivative of $\hat{\mathbf{v}}_{f_{pred}}$ should have the form of a cross product $\dot{\hat{\mathbf{v}}}_{f_{pred}} = \boldsymbol{\omega}_f \times \hat{\mathbf{v}}_{f_{pred}}$ for some angular velocity $\boldsymbol{\omega}_f$ which represents the rotation of $\hat{\mathbf{v}}_{f_{pred}}$. The purpose of designing the bias angular velocity command $\boldsymbol{\omega}_{bias}$ is to produce the angular velocity $\boldsymbol{\omega}_f$ that contributes to the alignment of $\hat{\mathbf{v}}_{f_{pred}}$ with $\hat{\mathbf{v}}_{f_d}$. To this end, an expression relating $\boldsymbol{\omega}_f$ to $\boldsymbol{\omega}_{bias}$ and other quantities is necessary. The following lemma summarises the vector-form expressions for the time-derivatives of σ and $\hat{\mathbf{k}}$. Note from Lemma 3 that the result of derivation will bring the relation in the form of $\dot{\hat{\mathbf{k}}} = \boldsymbol{\omega}_k \times \hat{\mathbf{k}}$ where $\boldsymbol{\omega}_k$ refers to the angular velocity of $\hat{\mathbf{k}}$.

Lemma 4 (Time-Derivatives of Three-Dimensional Lead Angle and Normal Vector of Manoeuvre Plane)**.**

$$\dot{\sigma} = \left\{(N-1)\,\boldsymbol{\omega}_r^{r\perp} + \boldsymbol{\omega}_{bias}\right\} \cdot \hat{\mathbf{k}} \tag{23}$$

$$\dot{\hat{\mathbf{k}}} = \frac{\boldsymbol{\omega}_{bias} \cdot \left(\hat{\mathbf{v}} \times \hat{\mathbf{k}}\right)}{\|\hat{\mathbf{r}} \times \hat{\mathbf{v}}\|} \hat{\mathbf{r}} \times \hat{\mathbf{k}} \tag{24}$$

Proof. Considering the definition of σ described in Sec. III-A, Eq. (10) defining $\hat{\mathbf{k}}$ can be rewritten as

$$\sin\sigma \hat{\mathbf{k}} = \hat{\mathbf{r}} \times \hat{\mathbf{v}} \tag{25}$$

Differentiating each side of Eq. (25) followed by substitution of Eqs. (11) and (20) along with application of Eq. (3) and the fact $\boldsymbol{\omega}_r^{r\perp} \perp \hat{\mathbf{v}}$ gives

$$\begin{aligned} \cos\sigma\dot{\sigma}\hat{\mathbf{k}} + \sin\sigma\dot{\hat{\mathbf{k}}} &= \dot{\hat{\mathbf{r}}} \times \hat{\mathbf{v}} + \hat{\mathbf{r}} \times \dot{\hat{\mathbf{v}}} \\ &= \left(\boldsymbol{\omega}_r^{r\perp} \times \hat{\mathbf{r}}\right) \times \hat{\mathbf{v}} + \hat{\mathbf{r}} \times (\boldsymbol{\omega}_v \times \hat{\mathbf{v}}) \\ &= (\hat{\mathbf{r}} \cdot \hat{\mathbf{v}}) \left(\boldsymbol{\omega}_v - \boldsymbol{\omega}_r^{r\perp}\right) - (\hat{\mathbf{r}} \cdot \boldsymbol{\omega}_v)\,\hat{\mathbf{v}} \\ &= (\hat{\mathbf{r}} \cdot \hat{\mathbf{v}}) \left\{(N-1)\,\boldsymbol{\omega}_r^{r\perp} + \boldsymbol{\omega}_{bias}\right\} - (\hat{\mathbf{r}} \cdot \boldsymbol{\omega}_{bias})\,\hat{\mathbf{v}} \end{aligned} \tag{26}$$

Lemma 3 states that $\hat{\mathbf{k}} \perp \dot{\hat{\mathbf{k}}}$, therefore, the expressions for $\dot{\sigma}$ and $\dot{\hat{\mathbf{k}}}$ can be found by taking the component of Eq. (26) in the direction parallel and perpendicular to $\hat{\mathbf{k}}$, respectively.

First, the dot product of Eq. (26) and $\hat{\mathbf{k}}$ gives

$$\cos\sigma\dot{\sigma} = (\hat{\mathbf{r}} \cdot \hat{\mathbf{v}}) \left(\boldsymbol{\omega}_v - \boldsymbol{\omega}_r^{r\perp}\right) \cdot \hat{\mathbf{k}} = (\hat{\mathbf{r}} \cdot \hat{\mathbf{v}}) \left\{(N-1)\,\boldsymbol{\omega}_r^{r\perp} + \boldsymbol{\omega}_{bias}\right\} \cdot \hat{\mathbf{k}} \tag{27}$$

since $\hat{\mathbf{k}} \perp \hat{\mathbf{v}}$ by definition. Then, using the relation $\cos\sigma = \hat{\mathbf{r}} \cdot \hat{\mathbf{v}}$ in Eq. (27) leads to Eq. (23).

Next, subtracting the component along $\hat{\mathbf{k}}$ from both sides of Eq. (26) while considering $\left(\boldsymbol{\omega}_r^{r\perp} \cdot \hat{\mathbf{k}}\right) \hat{\mathbf{k}} = \boldsymbol{\omega}_r^{r\perp}$, we have

$$\sin\sigma\dot{\hat{\mathbf{k}}} = \hat{\mathbf{r}} \times (\boldsymbol{\omega}_{bias} \times \hat{\mathbf{v}}) - (\hat{\mathbf{r}} \cdot \hat{\mathbf{v}}) \left(\boldsymbol{\omega}_{bias} \cdot \hat{\mathbf{k}}\right) \hat{\mathbf{k}} \tag{28}$$

The tuple of unit vectors $\left(\hat{\mathbf{v}}, \hat{\mathbf{k}}, \hat{\mathbf{v}} \times \hat{\mathbf{k}}\right)$ forms an orthonormal basis of $\mathbb{R}^3$, validating the expansion $\boldsymbol{\omega}_{bias} = (\boldsymbol{\omega}_{bias} \cdot \hat{\mathbf{v}})\,\hat{\mathbf{v}} + \left(\boldsymbol{\omega}_{bias} \cdot \hat{\mathbf{k}}\right) \hat{\mathbf{k}} + \left(\boldsymbol{\omega}_{bias} \cdot \left(\hat{\mathbf{v}} \times \hat{\mathbf{k}}\right)\right) \hat{\mathbf{v}} \times \hat{\mathbf{k}}$. Substituting the resolved form into Eq. (28) gives the following simplified expression.

$$\begin{aligned} \sin\sigma\dot{\hat{\mathbf{k}}} &= \hat{\mathbf{r}} \times \left[\left\{(\boldsymbol{\omega}_{bias} \cdot \hat{\mathbf{v}})\,\hat{\mathbf{v}} + \left(\boldsymbol{\omega}_{bias} \cdot \hat{\mathbf{k}}\right) \hat{\mathbf{k}} + \left(\boldsymbol{\omega}_{bias} \cdot \left(\hat{\mathbf{v}} \times \hat{\mathbf{k}}\right)\right) \hat{\mathbf{v}} \times \hat{\mathbf{k}}\right\} \times \hat{\mathbf{v}}\right] - (\hat{\mathbf{r}} \cdot \hat{\mathbf{v}}) \left(\boldsymbol{\omega}_{bias} \cdot \hat{\mathbf{k}}\right) \hat{\mathbf{k}} \\ &= \left(\boldsymbol{\omega}_{bias} \cdot \left(\hat{\mathbf{v}} \times \hat{\mathbf{k}}\right)\right) \hat{\mathbf{r}} \times \hat{\mathbf{k}} \end{aligned} \tag{29}$$

Rearranging Eq. (29) using the relation $\sin\sigma = \|\hat{\mathbf{r}} \times \hat{\mathbf{v}}\|$ results in Eq. (24). □

Now, the time-derivative of the second equality in Eq. (19) can be obtained by using Eq. (11) and the results of Lemma 4 along with repeated application Eq. (3) as

$$\begin{aligned}\dot{\hat{\mathbf{v}}}_{f_{pred}} &= \dot{\hat{\mathbf{r}}}\cos\left(\frac{1}{N-1}\sigma\right) - \hat{\mathbf{r}}\sin\left(\frac{1}{N-1}\sigma\right)\frac{1}{N-1}\dot{\sigma} \\ &\quad - \left(\dot{\hat{\mathbf{k}}}\times\hat{\mathbf{r}} + \hat{\mathbf{k}}\times\dot{\hat{\mathbf{r}}}\right)\sin\left(\frac{1}{N-1}\sigma\right) - \left(\hat{\mathbf{k}}\times\hat{\mathbf{r}}\right)\cos\left(\frac{1}{N-1}\sigma\right)\frac{1}{N-1}\dot{\sigma} \\ &= -\cos\left(\frac{1}{N-1}\sigma\right)\frac{\boldsymbol{\omega}_{bias}\cdot\hat{\mathbf{k}}}{N-1}\hat{\mathbf{k}}\times\hat{\mathbf{r}} - \sin\left(\frac{1}{N-1}\sigma\right)\left(\frac{\boldsymbol{\omega}_{bias}\cdot\left(\hat{\mathbf{v}}\times\hat{\mathbf{k}}\right)}{\|\hat{\mathbf{r}}\times\hat{\mathbf{v}}\|}\hat{\mathbf{k}} + \frac{\boldsymbol{\omega}_{bias}\cdot\hat{\mathbf{k}}}{N-1}\hat{\mathbf{r}}\right)\end{aligned} \tag{30}$$

Considering the relations $\hat{\mathbf{r}}\times\left(\hat{\mathbf{k}}\times\hat{\mathbf{r}}\right) = \hat{\mathbf{k}}$ and $\hat{\mathbf{k}}\times\left(\hat{\mathbf{k}}\times\hat{\mathbf{r}}\right) = -\hat{\mathbf{r}}$, Eq. (30) can be further simplified as

$$\begin{aligned}\dot{\hat{\mathbf{v}}}_{f_{pred}} &= \left\{\frac{\boldsymbol{\omega}_{bias}\cdot\left(\hat{\mathbf{v}}\times\hat{\mathbf{k}}\right)}{\|\hat{\mathbf{r}}\times\hat{\mathbf{v}}\|}\hat{\mathbf{r}} - \frac{\boldsymbol{\omega}_{bias}\cdot\hat{\mathbf{k}}}{N-1}\hat{\mathbf{k}}\right\}\times\left\{\hat{\mathbf{r}}\cos\left(\frac{1}{N-1}\sigma\right) - \left(\hat{\mathbf{k}}\times\hat{\mathbf{r}}\right)\sin\left(\frac{1}{N-1}\sigma\right)\right\} \\ &= \left\{\frac{\boldsymbol{\omega}_{bias}\cdot\left(\hat{\mathbf{v}}\times\hat{\mathbf{k}}\right)}{\|\hat{\mathbf{r}}\times\hat{\mathbf{v}}\|}\hat{\mathbf{r}} - \frac{\boldsymbol{\omega}_{bias}\cdot\hat{\mathbf{k}}}{N-1}\hat{\mathbf{k}}\right\}\times\hat{\mathbf{v}}_{f_{pred}}\end{aligned} \tag{31}$$

The final result of derivation confirms that it has the form of $\dot{\hat{\mathbf{v}}}_{f_{pred}} = \boldsymbol{\omega}_f\times\hat{\mathbf{v}}_{f_{pred}}$ with

$$\begin{aligned}\boldsymbol{\omega}_f &\triangleq \frac{\boldsymbol{\omega}_{bias}\cdot\left(\hat{\mathbf{v}}\times\hat{\mathbf{k}}\right)}{\|\hat{\mathbf{r}}\times\hat{\mathbf{v}}\|}\hat{\mathbf{r}} - \frac{\boldsymbol{\omega}_{bias}\cdot\hat{\mathbf{k}}}{N-1}\hat{\mathbf{k}} + \Omega\hat{\mathbf{v}}_{f_{pred}} \\ &= \left\{\frac{\boldsymbol{\omega}_{bias}\cdot\left(\hat{\mathbf{v}}\times\hat{\mathbf{k}}\right)}{\|\hat{\mathbf{r}}\times\hat{\mathbf{v}}\|} + \Omega\cos\left(\frac{1}{N-1}\sigma\right)\right\}\hat{\mathbf{r}} - \frac{\boldsymbol{\omega}_{bias}\cdot\hat{\mathbf{k}}}{N-1}\hat{\mathbf{k}} - \Omega\sin\left(\frac{1}{N-1}\sigma\right)\left(\hat{\mathbf{k}}\times\hat{\mathbf{r}}\right)\end{aligned} \tag{32}$$

for some $\Omega\in\mathbb{R}$. It is worth noting that the component along $\hat{\mathbf{k}}$ is responsible for rotation of $\hat{\mathbf{v}}_{f_{pred}}$ in the manoeuvre plane. The component of $\boldsymbol{\omega}_f$ parallel to $\hat{\mathbf{r}}$ arises from the rotation of manoeuvre plane, and it is indeed identical to the angular velocity of $\hat{\mathbf{k}}$, i.e., $\boldsymbol{\omega}_k$, as it can be observed from Eq. (31). The component $\Omega\hat{\mathbf{v}}_{f_{pred}}$ is included in Eq. (32) with the intention to represent the ambiguity in the redundant direction since the cross product operation removes the effect of parallel component.

Finally, the dynamics of the error angle e depicted in Fig. 2 can be related with $\boldsymbol{\omega}_{bias}$ using Eq. (31). Let $e \triangleq \cos^{-1}\left(\hat{\mathbf{v}}_{f_{pred}}\cdot\hat{\mathbf{v}}_{f_d}\right)$. Then, differentiating with respect to time and using Eq. (1) gives

$$\begin{aligned}\dot{e} &= -\frac{\dot{\hat{\mathbf{v}}}_{f_{pred}}\cdot\hat{\mathbf{v}}_{f_d}}{\sqrt{1-\left(\hat{\mathbf{v}}_{f_{pred}}\cdot\hat{\mathbf{v}}_{f_d}\right)^2}} = -\frac{\hat{\mathbf{v}}_{f_d}\cdot\left(\boldsymbol{\omega}_f\times\hat{\mathbf{v}}_{f_{pred}}\right)}{\left\|\hat{\mathbf{v}}_{f_{pred}}\times\hat{\mathbf{v}}_{f_d}\right\|} \\ &= -\boldsymbol{\omega}_f\cdot\frac{\hat{\mathbf{v}}_{f_{pred}}\times\hat{\mathbf{v}}_{f_d}}{\left\|\hat{\mathbf{v}}_{f_{pred}}\times\hat{\mathbf{v}}_{f_d}\right\|}\end{aligned} \tag{33}$$

Equation (33) clearly indicates that the component of $\boldsymbol{\omega}_f$ in the direction of $\hat{\mathbf{v}}_{f_{pred}}\times\hat{\mathbf{v}}_{f_d}$ contributes to time-variation of e.

D. Design of Bias Angular Velocity Command

The bias angular velocity command $\boldsymbol{\omega}_{bias}$ should be designed to rotate $\hat{\mathbf{v}}_{f_{pred}}$ as desired. More specifically, $\boldsymbol{\omega}_{bias}$ needs to be designed so that the resulting $\boldsymbol{\omega}_f$ produces the required amount of rotation about the axis $\frac{\hat{\mathbf{v}}_{f_{pred}} \times \hat{\mathbf{v}}_{f_d}}{\left\| \hat{\mathbf{v}}_{f_{pred}} \times \hat{\mathbf{v}}_{f_d} \right\|}$. The minimal movement of $\hat{\mathbf{v}}_{f_{pred}}$ in the shortest path to the fixed vector $\hat{\mathbf{v}}_{f_d}$ is the rotation about a fixed axis perpendicular to the plane of span $\left(\hat{\mathbf{v}}_{f_{pred}}, \hat{\mathbf{v}}_{f_d} \right)$. Rotation of $\hat{\mathbf{v}}_{f_{pred}}$ around $\hat{\mathbf{v}}_{f_d}$ can be used for trajectory shaping purposes at the expense of increased magnitude of $\boldsymbol{\omega}_f$ which will require additional control effort in $\boldsymbol{\omega}_{bias}$.

The design process begins with specifying $\boldsymbol{\omega}_{f_d}$ that encodes the desired motion of $\hat{\mathbf{v}}_{f_{pred}}$ as the virtual control input, and proceeds with conversion into the real control input $\boldsymbol{\omega}_{bias}$. Motivated by the observations of Eq. (33), the virtual control input can be constructed as

$$\boldsymbol{\omega}_{f_d} = k_e\left(r\right) \left|\dot{r}\right| e \frac{\hat{\mathbf{v}}_{f_{pred}} \times \hat{\mathbf{v}}_{f_d}}{\left\| \hat{\mathbf{v}}_{f_{pred}} \times \hat{\mathbf{v}}_{f_d} \right\|} + \Omega_\mu \hat{\mathbf{v}}_{f_d} \tag{34}$$

with a positive range-varying gain $k_e\left(r\right)$ and an angular rate Ω_μ in order to prescribe the desired closed-loop error dynamics as

$$\dot{e} = -k_e\left(r\right) \left|\dot{r}\right| e \tag{35}$$

Note that changing the independent variable of Eq. (35) from t to r leads to $e' = -k_e\left(r\right) \operatorname{sign}\left(\dot{r}\right) e$ where $\left(\cdot\right)' \triangleq \frac{d}{dr}\left(\cdot\right)$. Next, the ambiguity in Ω should be resolved to fully determine the real control input. This can be done by resolving $\boldsymbol{\omega}_f$ (and $\boldsymbol{\omega}_{f_d}$) in the Cartesian coordinate system with $\left(\hat{\mathbf{k}}, \hat{\mathbf{r}}, \hat{\mathbf{k}} \times \hat{\mathbf{r}} \right)$ as the basis vectors. By equating Eq. (32) with Eq. (34), taking the dot product with $\hat{\mathbf{k}} \times \hat{\mathbf{r}}$, and rearranging the result about Ω, we have

$$\Omega = -\frac{\boldsymbol{\omega}_{f_d} \cdot \left(\hat{\mathbf{k}} \times \hat{\mathbf{r}} \right)}{\sin\left(\frac{1}{N-1}\sigma \right)} \tag{36}$$

After back substitution of Eq. (36), the dot products of Eq. (32) with $\hat{\mathbf{r}}$ and $\hat{\mathbf{k}}$ can be written as

$$\frac{\boldsymbol{\omega}_{bias} \cdot \left(\hat{\mathbf{v}} \times \hat{\mathbf{k}} \right)}{\left\| \hat{\mathbf{r}} \times \hat{\mathbf{v}} \right\|} - \boldsymbol{\omega}_{f_d} \cdot \left(\hat{\mathbf{k}} \times \hat{\mathbf{r}} \right) \cot\left(\frac{1}{N-1}\sigma \right) = \boldsymbol{\omega}_{f_d} \cdot \hat{\mathbf{r}} \tag{37}$$

$$-\frac{\boldsymbol{\omega}_{bias} \cdot \hat{\mathbf{k}}}{N-1} = \boldsymbol{\omega}_{f_d} \cdot \hat{\mathbf{k}} \tag{38}$$

The component of $\boldsymbol{\omega}_{bias}$ in the direction of $\hat{\mathbf{v}}$ does not generate any normal acceleration for steering of $\hat{\mathbf{v}}$. This implies that a $\boldsymbol{\omega}_{bias}$ having components only in $\hat{\mathbf{k}}$ and $\hat{\mathbf{v}} \times \hat{\mathbf{k}}$ suffices our control design objective. Therefore, the bias angular velocity command that produces the desired angular velocity of the predicted final velocity direction can be fully determined from Eqs. (37)-(38) as follows:

$$\boldsymbol{\omega}_{bias} = -\left(N-1\right) \left(\boldsymbol{\omega}_{f_d} \cdot \hat{\mathbf{k}} \right) \hat{\mathbf{k}} + \sin\sigma \, \boldsymbol{\omega}_{f_d} \cdot \left\{ \hat{\mathbf{r}} + \cot\left(\frac{1}{N-1}\sigma \right) \left(\hat{\mathbf{k}} \times \hat{\mathbf{r}} \right) \right\} \left(\hat{\mathbf{v}} \times \hat{\mathbf{k}} \right) \tag{39}$$

Remark 1 (Corner Cases).

The unit vector in the direction of $\hat{\mathbf{v}}_{f_{pred}} \times \hat{\mathbf{v}}_{f_d}$ that enters into the $\boldsymbol{\omega}_{f_d}$ of Eq. (34) is well-defined as long as $\hat{\mathbf{v}}_{f_{pred}} \neq \pm\hat{\mathbf{v}}_{f_d}$. The two corner cases due to the parallel pairs of $\left(\hat{\mathbf{v}}_{f_{pred}}, \hat{\mathbf{v}}_{f_d}\right)$ are not considerably restricting the applicability of proposed guidance law in practice as they can be reasonably mitigated by an appropriate exception handling or a design modification for more reliability.

The first case of $\hat{\mathbf{v}}_{f_{pred}} = \hat{\mathbf{v}}_{f_d}$, which is equivalent to $e = 0$, corresponds to the situation when the vehicle employing only the PPNG will arrive at the target with the desired direction. This case does not incur a serious problem in practice because a bias command is not necessary to turn $\hat{\mathbf{v}}_{f_{pred}}$. Therefore, setting the first term in Eq. (34) to be zero suffices our purpose. Also, this case does not involve a mathematical singularity in Eq. (34), since L'Hôpital's rule indicates that $\lim_{e\to 0^+} \frac{e}{\left\|\hat{\mathbf{v}}_{f_{pred}} \times \hat{\mathbf{v}}_{f_d}\right\|} = \lim_{e\to 0^+} \frac{e}{\sin e} = \lim_{e\to 0^+} \frac{1}{\cos e} = 1$.

The other case of $\hat{\mathbf{v}}_{f_{pred}} = -\hat{\mathbf{v}}_{f_d}$, which is equivalent to $e = \pi$, corresponds to the situation when the direction of rotation for $\hat{\mathbf{v}}_{f_{pred}}$ cannot be uniquely determined due to the infinitude of possible solutions. In this exceptional case, the angular velocity $\boldsymbol{\omega}_{f_d}$ in any direction on the plane perpendicular to $\hat{\mathbf{v}}_{f_d}$ will reduce e. In view of the finite-time monotonic convergence of e guaranteed by the proposed method, one practical remedy is to simply avoid initialisation at $e = \pi$. Another possible solution is to apply an arbitrarily small perturbation in $\boldsymbol{\omega}_{f_d}$ to escape from the point of $e = \pi$. Also, the singularity can be avoided by modifying the design as $\boldsymbol{\omega}_{f_d} = k_e(r)\,|\dot{r}|\, e\hat{\mathbf{v}}_{f_{pred}} \times \hat{\mathbf{v}}_{f_d} + \Omega_\mu \hat{\mathbf{v}}_{f_d}$ at the expense of the closed-loop error dynamics becoming a nonlinear asymptotically convergent system $e' = -k_e(r)\,\mathrm{sign}(\dot{r})\, e \sin e$.

Remark 2 (Effects of Nonideal Acceleration Tracking Response).

Performance degradation in terms of larger miss distance or impact angle error is generally expected in the presence of a lag-like dynamics in the lateral acceleration responding to the command. Nevertheless, the lag in the tracking response will impact the result to a limited extent in stationary target interception when the convergence of e to zero over time is fast enough to require only a small correction near the end of engagement and the terminal acceleration command as well as its rate smoothly approaches zero. One can prescribe the desired convergence patterns through judicious choice of design parameters.

Remark 3 (Extension to Control of Impact Angle against Manoeuvring Target).

The proposed BPNG can be extended to the case of intercepting a manoeuvring target with the impact angle constraint by formulating the problem in the relative frame where target remains fixed and applying the same derivation procedure. The notion of design first in the relative frame followed by realisation in the absolute frame has been employed in [24] in a similar manner.

E. Consideration of Shaping Requirements for Choice of Design Parameters

The proposed design approach introduces N, $k_e(r)$, and Ω_μ as the design parameters that should be selected to reflect the trajectory shaping requirements. The navigation ratio N can be reasonably chosen a priori considering the baseline performance. The other design parameters are mainly associated with the rotation of $\hat{\mathbf{v}}_{f_{pred}}$ as well as the rotation of manoeuvre plane.

1) Design of $k_e(r)$: The function $k_e(r)$ can be selected by considering the scalar linear closed-loop error dynamics given by Eq. (35) to prescribe a desired convergence pattern in the response of e which can be expressed as

$$e(r) = e(r_0) \exp\left[\int_{r_0}^{r} k_e(\rho)\, d\rho\right] \tag{40}$$

Finite-time convergence of the error requires choosing $k_e(r)$ so that the solution in Eq. (40) satisfies $e(r) = 0$ in $r \in [0, r_c]$ for some $r_c \geq 0$. Moreover, the previous studies such as [50] provided an alternative way to choose $k_e(r)$ by solving an optimal control problem formulated as

$$\begin{aligned} \underset{\boldsymbol{\omega}_f}{\text{minimise}} \qquad & J = \int_0^r W(\rho) \left\| \frac{\boldsymbol{\omega}_f(\rho)}{\dot{r}} \right\|^p d\rho \\ \text{subject to} \quad & e'(r) = -\frac{\boldsymbol{\omega}_f(r)}{\dot{r}} \cdot \frac{\hat{\mathbf{v}}_{f_{pred}} \times \hat{\mathbf{v}}_{f_d}}{\left\| \hat{\mathbf{v}}_{f_{pred}} \times \hat{\mathbf{v}}_{f_d} \right\|} \\ & e(0) = 0 \end{aligned} \tag{41}$$

where $p \in (0, \infty)$ and $W(\rho)$ is a weighting function that attains positive value in the interval $[0, r]$. The optimal solution satisfies

$$k_e(r) = \frac{W^{-\frac{1}{p-1}}(r)}{\int_0^r W^{-\frac{1}{p-1}}(\rho)\, d\rho} \tag{42}$$

One representative example placing a larger weight on the region of smaller r for suppression of rotation in the latter part of engagement is to take $p = 2$ and $W(r) = r^{-n}$ where $n \geq 0$, the choice that results in

$$k_e(r) = \frac{n+1}{r} \tag{43}$$

Substituting the feedback gain given by Eq. (43) into Eqs. (40) and (34) with $\Omega_\mu = 0$ gives the solution for the closed-loop error trajectory and the magnitude of the desired angular velocity in terms of r as

$$e(r) = e(r_0) \left(\frac{r}{r_0}\right)^{n+1} \tag{44}$$

$$\left\| \boldsymbol{\omega}_{f_d} \right\| = (n+1) \left| \dot{r} \right| e(r_0) \frac{r^n}{{r_0}^{n+1}} \tag{45}$$

2) Design of Ω_μ: Obviously, $\Omega_\mu = 0$ is the choice to make the predicted rotation of $\hat{\mathbf{v}}_{f_{pred}}$ follow the shortest possible path for regulation of e. Nonzero Ω_μ does not contribute to reduction of e. Nonetheless, the additional degree-of-freedom for roll-like motion of the predicted final velocity around the desired arrival direction can be utilised for objectives that are independent from satisfying the terminal direction constraint. One example is to deliberately induce weaving patterns for enhancing survivability and target observability while guaranteeing satisfaction of the terminal direction constraint. One possible design for inducing a barrel roll type evasive manoeuvre is to resemble the BPNG presented in [18], except that the previous study does not consider a specific direction for incidence to the target. This can be done by using Ω_μ with its magnitude given by a monotonically increasing function of r such as

$$\Omega_\mu = \Omega_{\mu_0} \left(\frac{r}{r_0} \right)^m \tag{46}$$

with $\Omega_{\mu_0} \neq 0$ and $m \geq 0$. Other types of functions such as sinusoidal, square, triangular, sawtooth waveforms or random sequences can also be chosen as Ω_μ to generate erratic manoeuvre patterns without loss of convergence in e.

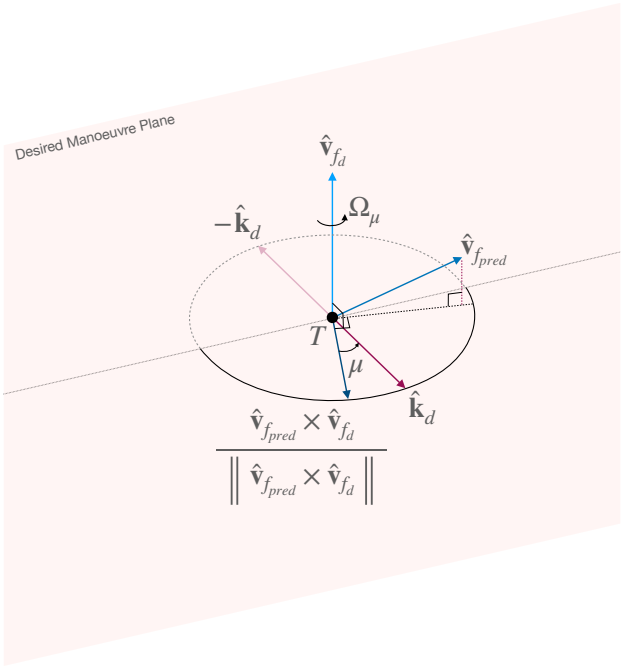

Fig. 3: Desired Manoeuvre Plane and Rotation Around Desired Arrival Direction

Another example is to place the manoeuvre plane in a desired orientation. Suppose that the unit normal vector of the desired manoeuvre plane is given by $\hat{\mathbf{k}}_{plane}$. The manoeuvre plane is said to be aligned with the desired orientation if the trace of $\hat{\mathbf{v}}_{f_{pred}}$ approaching $\hat{\mathbf{v}}_{f_d}$ lies in the desired manoeuvre plane,

or equivalently, the plane spanned by $\hat{\mathbf{v}}_{f_{pred}}$ and $\hat{\mathbf{v}}_{f_d}$ matches the desired one. Therefore, manoeuvre plane alignment can be achieved when the rotational axis for convergence of $\hat{\mathbf{v}}_{f_{pred}}$ toward $\hat{\mathbf{v}}_{f_d}$, which is represented by $\frac{\hat{\mathbf{v}}_{f_{pred}} \times \hat{\mathbf{v}}_{f_d}}{\left\| \hat{\mathbf{v}}_{f_{pred}} \times \hat{\mathbf{v}}_{f_d} \right\|}$, is parallel to $\pm \hat{\mathbf{k}}_{plane}$.

One should take the desired rotational axis $\hat{\mathbf{k}}_d$ among two possible directions $\pm \hat{\mathbf{k}}_{plane}$ by the one closer to the current rotational axis to produce smaller amount of correction effort. To this end, the desired rotational axis can be defined as

$$\hat{\mathbf{k}}_d \triangleq \text{sign}\left(\left(\hat{\mathbf{v}}_{f_{pred}} \times \hat{\mathbf{v}}_{f_d} \right) \cdot \hat{\mathbf{k}}_{plane} \right) \hat{\mathbf{k}}_{plane} \tag{47}$$

Then, the manoeuvre plane alignment error angle $\mu \in \left[-\frac{\pi}{2}, \frac{\pi}{2} \right]$ can be defined as

$$\begin{aligned} \mu &\triangleq \text{atan2}\left[\left\{ \left(\hat{\mathbf{v}}_{f_{pred}} \times \hat{\mathbf{v}}_{f_d} \right) \times \hat{\mathbf{k}}_d \right\} \cdot \hat{\mathbf{v}}_{f_d}, \ \left(\hat{\mathbf{v}}_{f_{pred}} \times \hat{\mathbf{v}}_{f_d} \right) \cdot \hat{\mathbf{k}}_d \right] \\ &= \text{atan2}\left[\left(\hat{\mathbf{v}}_{f_{pred}} \times \hat{\mathbf{v}}_{f_d} \right) \cdot \left(\hat{\mathbf{k}}_d \times \hat{\mathbf{v}}_{f_d} \right), \ \left(\hat{\mathbf{v}}_{f_{pred}} \times \hat{\mathbf{v}}_{f_d} \right) \cdot \hat{\mathbf{k}}_d \right] \end{aligned} \tag{48}$$

The quantities $\hat{\mathbf{k}}_d$ and μ depicted in Fig. 3 is consistent with Eqs. (47) and (48), respectively.

Alignment of manoeuvre plane can be achieved by employing a Ω_μ that nullifies μ. Note that μ defined in Eq. (48) verifies the relations $\frac{\hat{\mathbf{v}}_{f_{pred}} \times \hat{\mathbf{v}}_{f_d}}{\left\| \hat{\mathbf{v}}_{f_{pred}} \times \hat{\mathbf{v}}_{f_d} \right\|} \times \hat{\mathbf{k}}_d = \sin\mu \hat{\mathbf{v}}_{f_d}$ and $\frac{\hat{\mathbf{v}}_{f_{pred}} \times \hat{\mathbf{v}}_{f_d}}{\left\| \hat{\mathbf{v}}_{f_{pred}} \times \hat{\mathbf{v}}_{f_d} \right\|} \cdot \hat{\mathbf{k}}_d = \cos\mu$. The relation $\dot{\mu} = -\Omega_\mu$ holds with the angular rate Ω_μ defined to be positive for rotation of $\hat{\mathbf{v}}_{f_{pred}}$ with respect to $\hat{\mathbf{v}}_{f_d}$ according to the right-hand rule. Therefore, the angular rate command given by

$$\Omega_\mu = k_\mu(r) |\dot{r}| \mu \tag{49}$$

with a positive range-varying gain $k_\mu(r)$ specifies the closed-loop dynamics of μ for the case of $\dot{r} \leq 0$ as

$$\mu' = k_\mu(r) \mu \tag{50}$$

By following the similar reasoning as explained above, the command given in Eq. (49) with the gain given by

$$k_\mu(r) = \frac{W^{-\frac{1}{p-1}}(r)}{\int_0^r W^{-\frac{1}{p-1}}(\rho) d\rho} \tag{51}$$

where $p \in (0, \infty)$ and $W(\rho) > 0$ is the optimal control solution to the following problem.

$$\begin{aligned} \underset{\Omega_\mu}{\text{minimise}} \quad & J = \int_0^r W(\rho) \left\| \frac{\Omega_\mu(\rho)}{\dot{r}} \right\|^p d\rho \\ \text{subject to} \quad & \mu'(r) = -\frac{\Omega_\mu(r)}{\dot{r}} \\ & \mu(0) = 0 \end{aligned} \tag{52}$$

IV. Numerical Simulation

This section will illustrate the performance of the proposed guidance law with various scenarios. The simulation cases are divided according to the purpose as shown below:

- Case 1. To verify the basic performance with closed-loop trajectories for various desired arrival directions and to compare with an existing method
- Case 2. To show the effects of design parameter in the gain function on error convergence
- Case 3. To demonstrate the modification considering look angle restriction
- Case 4. To demonstrate the modification considering rotation of manoeuvre plane around desired arrival direction

TABLE I: Simulation Parameters

Parameter	Unit	Case 1	Case 2	Case 3	Case 4
$\mathbf{r}_M(t_0)$	m		$\begin{bmatrix}0 & 0 & 0\end{bmatrix}^T$		
$\mathbf{r}_T$	m		$\begin{bmatrix}10\,000 & 0 & 0\end{bmatrix}^T$		
$\mathbf{v}(t_0)$	m/s		$300\begin{bmatrix}\frac{1}{\sqrt{2}} & 0 & \frac{1}{\sqrt{2}}\end{bmatrix}^T$		
N	-		3		
γ_{f_d}	deg	-70	-70	-70	-90
χ_{f_d}	deg	$\{0, 45, 90, \cdots, 315\}$	180	225	180
n (in $k_e(r) = \frac{n+1}{r}$)	-	1	$\{0, 1, 2, 3, 4\}$	1	1
$\boldsymbol{\Omega}_\mu$	rad/s	0	0	0	Eqs. (46)*, (49)†
$f_{\text{act}}(\sigma)$	-	1	1	$\frac{2}{\pi}\cos^{-1}\left(\left(\frac{\sigma}{\sigma_{\text{lim}}}\right)^{100}\right)$	$\frac{2}{\pi}\cos^{-1}\left(\left(\frac{\sigma}{\sigma_{\text{lim}}}\right)^{4}\right)$
σ_{lim}	deg	-	-	$\{45, 50, 55, 60\}$	90

* $\boldsymbol{\Omega}_{\mu_0} = \{0, 0.1, 0.15, 0.2, 0.25\}$, $m = 3$

† $k_\mu(r) = \frac{21}{r}$, $\hat{\mathbf{k}}_d = \left\{\begin{bmatrix}1 & 0 & 0\end{bmatrix}^T, \begin{bmatrix}\frac{1}{\sqrt{2}} & \frac{1}{\sqrt{2}} & 0\end{bmatrix}^T, \begin{bmatrix}0 & 1 & 0\end{bmatrix}^T\right\}$

Table I summarises the parameter values considered for each simulation case. The initial position and velocity of the vehicle and the target position in Table I are represented in a fixed Cartesian coordinate system, and the desired arrival direction vector is represented in the same frame with vertical and horizontal flight path angles $(\gamma_{f_d}, \chi_{f_d})$ as $\hat{\mathbf{v}}_{f_d} = \begin{bmatrix}\cos\gamma_{f_d}\sin\chi_{f_d} & \cos\gamma_{f_d}\cos\chi_{f_d} & \sin\gamma_{f_d}\end{bmatrix}^T$. All simulation cases apply the range-varying gain $k_e(r)$ given by Eq. (43). In addition to demonstrating effectiveness of the proposed BPNG in achieving a range of terminal conditions, simulation Case 1 also compares the closed-loop performance with the quaternion-based three-dimensional impact-angle-control guidance law (QIACG) developed in [22]. Simulation Case 3 demonstrates the effectiveness of the

modification described in Appendix for maintaining the look angle within a prespecified limit. Simulation Case 4 illustrates the effect of manoeuvre plane rotation for two different algorithms developed in Sec. III-E for evasive guidance with arrival direction constraint and alignment with the desired orientation. The simulation model for the vehicle motion is a point mass kinematic model which maintains a constant speed and does not experience response lag in lateral acceleration.

A. Case 1. Performance for Various Desired Arrival Directions and Comparison with Existing Method

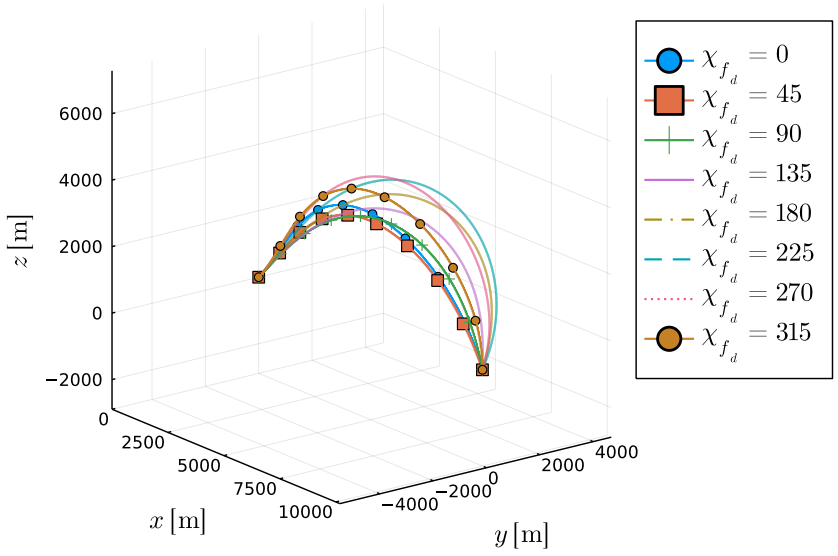

Fig. 4: Simulation Result for Case 1 – Three-Dimensional Trajectory

Figures 4-5 show the simulation results for Case 1. Figures 4, 5b, and 5c show that the missile successfully intercepts the target in all cases. The predicted final direction error e decreases monotonically to zero at the same time as shown in Fig. 5d, indicating the capability of the proposed BPNG to achieve various desired arrival directions. Figures 5e and 5f are the time histories for the magnitude of inputs that drive the convergence of heading error and impact direction error; the total lateral acceleration and the bias angular velocity command, respectively. The results for the command magnitudes are obviously identical for the symmetric desired arrival directions including the two-dimensional view of the trajectory shown in Fig. 5a, showing that the proposed BPNG enables a wide coverage of final conditions neither being unnecessarily sensitive nor giving preference to certain direction of rotation or manoeuvre plane. Also, the commands are smooth throughout the engagement and their final values are zero. Overall, the proposed BPNG exhibits good performance in satisfying the given constraints. A test based on a number

of numerical simulations indicates that the proposed BPNG provides a wide coverage of achievable missions.

The closed-loop performance is compared to the QIACG developed in [22] as an extension of the planar linear quadratic optimal guidance law. Assuming that the error angles are small enough to justify the validity of linearisation, the QIACG minimises the time-to-go weighted control energy given by

$$J = \frac{1}{2}\int_t^{t_f} \frac{\|\mathbf{a}\|^2}{{t_{go}}^{\nu}} d\tau \tag{53}$$

where $\nu \geq 0$ is the design parameter introduced to adjust the distribution of manoeuvre demand over time. The QIACG command can be expressed as

$$\mathbf{a}_{QIACG}^{v\perp} = \left(N_\sigma \boldsymbol{\omega}_r^{r\perp} + \frac{N_f}{t_{go}} \varepsilon \frac{\hat{\mathbf{v}}_{f_d} \times \hat{\mathbf{v}}}{\left\| \hat{\mathbf{v}}_{f_d} \times \hat{\mathbf{v}} \right\|} \right) \times \mathbf{v} \tag{54}$$

where

$$\begin{aligned} \varepsilon &= \cos^{-1}\left(\hat{\mathbf{v}}_{f_d} \cdot \hat{\mathbf{v}}\right), \qquad t_{go} \approx \frac{r}{-\dot{r}} \\ N_\sigma &= (\nu+2)(\nu+3), \qquad N_f = (\nu+1)(\nu+2) \end{aligned} \tag{55}$$

The definition of the arrival direction error differs between two guidance laws as e in the proposed BPNG is referenced to the predicted final velocity direction $\hat{\mathbf{v}}_{f_{pred}}$ whereas ε in the QIACG is referenced to the current velocity direction $\hat{\mathbf{v}}$. The performance index considered in [22] is closely related yet different from that of this study, and [22] took a substantially different design approach.

The design parameters n for the proposed BPNG and ν for the QIACG govern the trajectory characteristics through the power function weighting factor in the performance indices of Eqs. (41) and (53). Because of the apparent similarity between the performance indices, one can reasonably compare the characteristics of the guidance laws by prescribing a similar overall trend in the lateral acceleration through the choice of n and ν. The coefficient ν for the QIACG is chosen to have the same value as n for the proposed BPNG, i.e., $\nu = n = 1$.

Figure 6 shows the simulation results for the QIACG with the same simulation scenario. Table II compares the time-averaged total control consumption evaluated according to the metric defined by $\bar{A} = \frac{1}{t_f - t_0}\int_{t_0}^{t_f} \|\mathbf{a}\|\, d\tau$. The simulation results indicate that both guidance laws are capable of achieving interception while satisfying arrival direction constraint in three-dimensional space. However, the QIACG consumes more control effort than the proposed BPNG. The control expenditure difference between two guidance laws grows with the increase of initial error. The observed overspending of control action is thought to be attributed to the fact that baseline model prediction is out of consideration in the definition of arrival direction error used in the QIACG and the invalidity of small angle assumption that forms the basis of the QIACG.

TABLE II: Case 1 - Comparison of Time-Averaged Total Control Expenditure $\bar{A}$

$\lvert\chi_{fd} - \chi_0\rvert$ [deg]	Proposed BPNG [m/s^2]	QIACG [22] [m/s^2]
0	14.425	14.795
45	15.395	16.169
90	16.723	17.921
135	17.354	18.712
180	17.409	18.537

B. Case 2. Effect of Gain Coefficient

Figure 7 shows the simulation results for Case 2. The effect of gain coefficient n is apparent mainly in Fig. 7d as the tuning knob for the rate at which e converges to zero. A large gain leads to faster convergence at the cost of increased initial input as it can be seen from Fig. 7f. Figure 7d also shows that $\dot{e}$ becomes zero as well as e when $n \geq 1$. Also, the bias angular velocity command $\boldsymbol{\omega}_{bias}$ becomes zero at the end of engagement for $n \geq 1$. Figure 7f indicates that $n \geq 2$ is required to nullify the rate of ω_{f_d} and that of ω_{bias} as well at the final time. The tendency is understandable from the optimal control point of view that a larger n places an increasingly higher weight $W(r)$ as r decreases in the performance index J of Eq. (41). All these observations are consistent with the knowledge about the closed-loop system solutions derived in Eqs. (44) and (45). In summary, the design parameter determines the tradeoff between the rate of error convergence against the magnitude of initial command and the degree of smoothness in closed-loop trajectories. One can refer to the analytical predictions to choose the design parameter as needed in each mission.

C. Case 3. Consideration of Look Angle Restriction

Figure 8 shows the simulation results for Case 3. Figures 8b and 8d together show that the modified version of the proposed BPNG that includes a lead-angle-dependent bias command activation function $f_{\text{act}}(\sigma)$ successfully achieves impact-direction-constrained interception. Figure 8c clearly shows that the design modification proposed in Sec. III-E is effective in keeping the lead angle below the specified limit in each case. The velocity-vector-referenced lead angle is equivalent to the body-axis-referenced look angle under the assumption of zero angle-of-attack. In this sense, the simulation results suggest that a look angle restriction can be readily incorporated into the proposed BPNG framework.

D. Case 4. Consideration of Manoeuvre Plane Rotation

Figures 9 and 10 show the simulation results for Case 4 obtained by employing the proposed manoeuvre plane rotation algorithms given by Eqs. (46) and (49), respectively. Figure 9 shows that the missile performs additional rotational movement during its course to the target. A larger magnitude of Ω_μ leads to the increased amount of rotation enclosing the desired arrival direction. Also, the direction of the evasive rotation is determined by sign (Ω_μ) according to the right-hand rule. On the other hand, Figure 10 shows that the proposed BPNG adopting Eq. (49) enables the vehicle to take different manoeuvre planes as needed even for the same target position and desired arrival direction. The manoeuvre plane alignment error μ converges monotonically to zero as shown in Fig. 10d. In all examples considered in Case 4, the proposed BPNG achieves the basic guidance objectives of nullifying r and e regardless of a nonzero Ω_μ included in ω_{f_d}. This observation confirms the property discussed in Sec. III-E that the additional rotation of manoeuvre plane can be performed in a manner decoupled from the control of final velocity direction. The results support the extensibility of the proposed BPNG provided by the additional degree-of-freedom for manoeuvre plane rotation in contrast to the QIACG discussed in Case 1.

V. Conclusions

This study developed a new approach to construct three-dimensional Biased Proportional Navigation Guidance laws (BPNG) in vector form for arrival direction control and trajectory shaping based on the notion of predictive correction. The most effective axis for spatial rotation of the predicted final velocity vector for alignment with the desired direction was identified. Also, the way to realise such rotation of the future velocity vector with the corresponding angular velocity command for the current vehicle velocity vector was developed. The properties of the three-dimensional BPNG including convergence of the predicted final velocity direction error and possible design extensions considering various trajectory shaping goals were discussed. The proposed three-dimensional BPNG demanding no tangential acceleration is useful for many aircraft and missile applications as it has the advantage of being a simple-to-implement continuous feedback guidance method. The proposed method can remove ambiguities in the widely-adopted approach of arrival direction control by means of planar techniques applied to two orthogonal planes and avoid singularity issues. The three-dimensional BPNG is also useful to deal with in-flight change of target position or desired arrival direction as it naturally handles the change of manoeuvre plane. One unique benefit that distinguishes the three-dimensional BPNG from planar methods is that the proposed BPNG provides the rotational rate of predicted final velocity vector around the desired arrival direction as an additional degree-of-freedom for trajectory shaping which is decoupled from achievement of the terminal constraints.

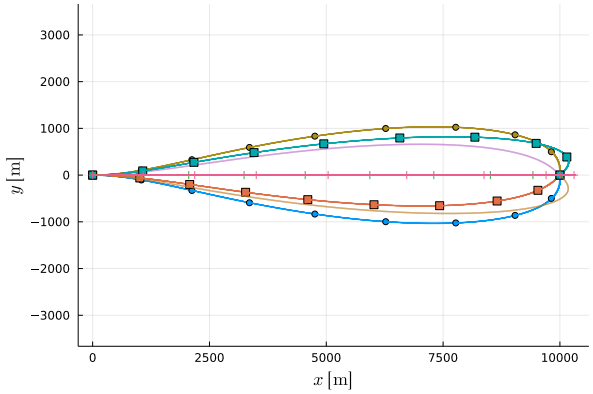

(a) Two-Dimensional Trajectory

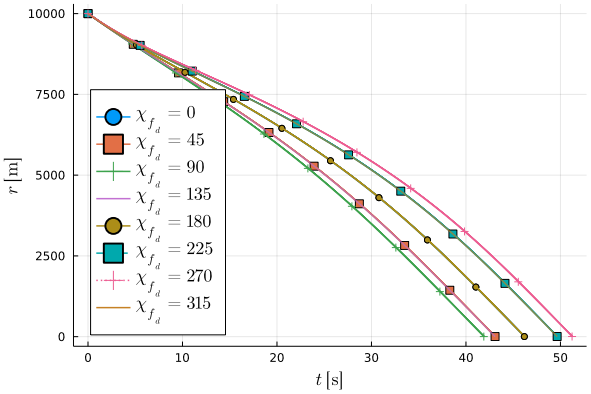

(b) Range

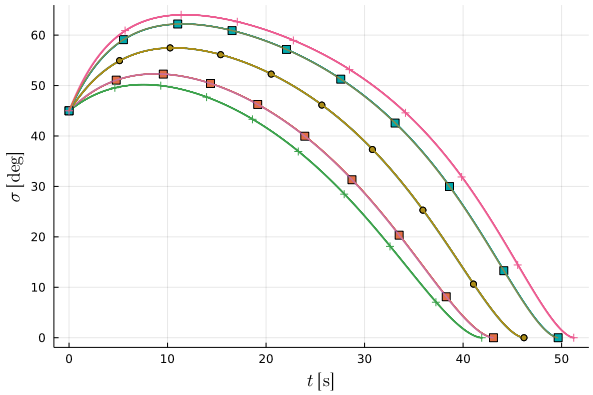

(c) Lead Angle

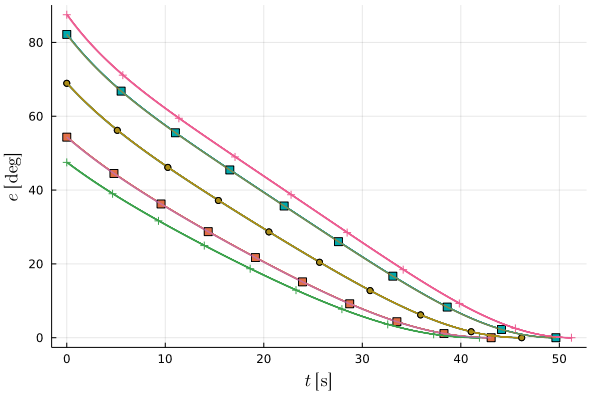

(d) Predicted Final Direction Error

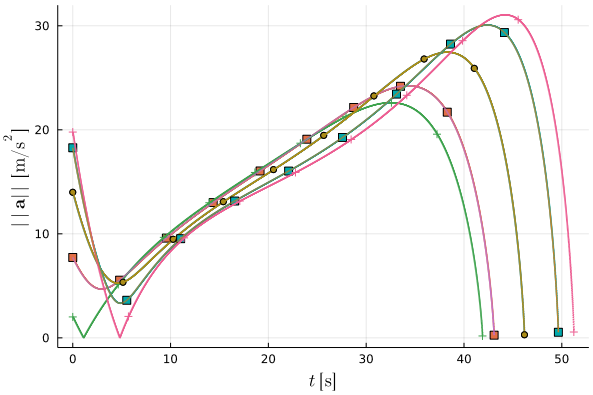

(e) Magnitude of Acceleration

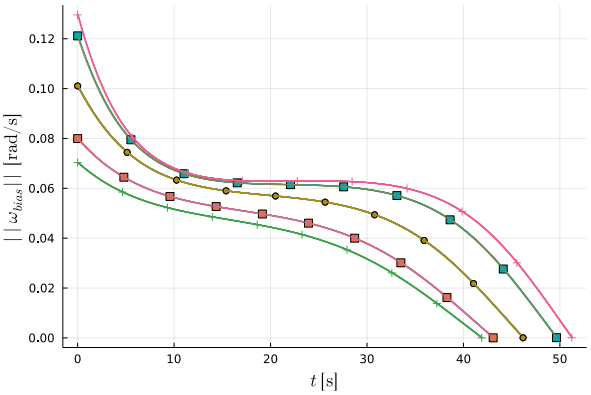

(f) Magnitude of Bias Angular Velocity Command

Fig. 5: Simulation Results for Case 1

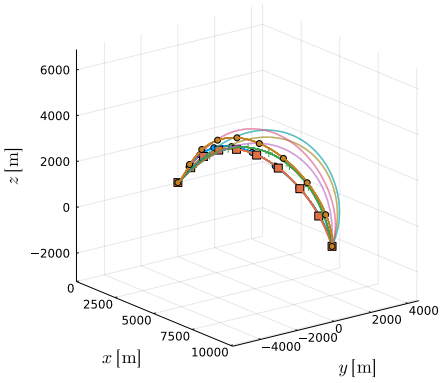

(a) Three-Dimensional Trajectory

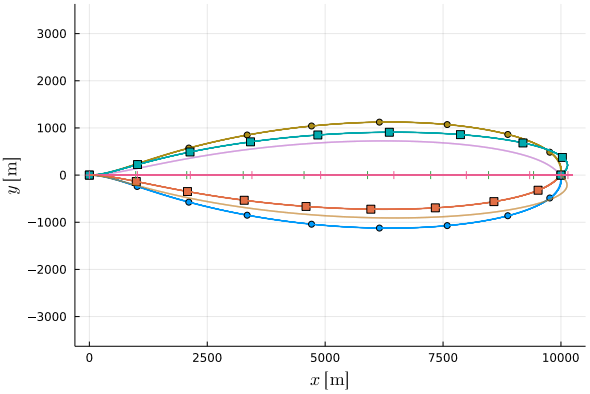

(b) Two-Dimensional Trajectory

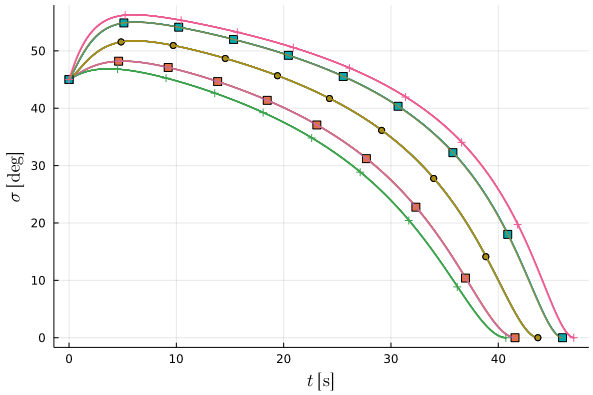

(c) Lead Angle

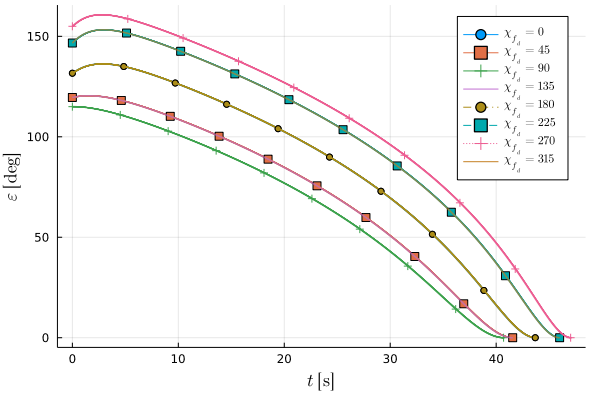

(d) Current Direction Error

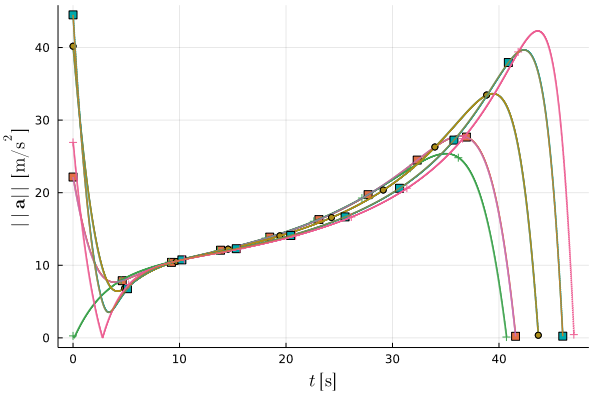

(e) Magnitude of Acceleration

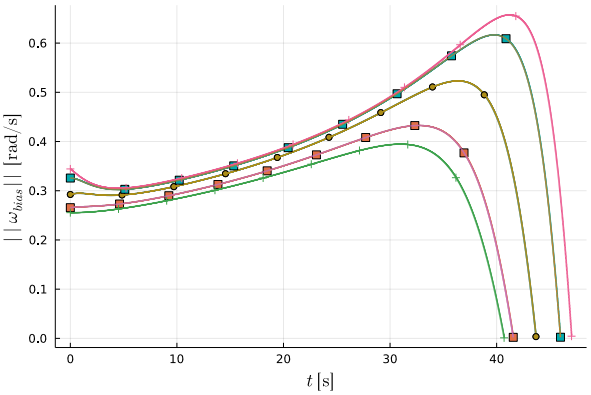

(f) Magnitude of Bias Angular Velocity Command

Fig. 6: Simulation Results for Case 1 with QIACG

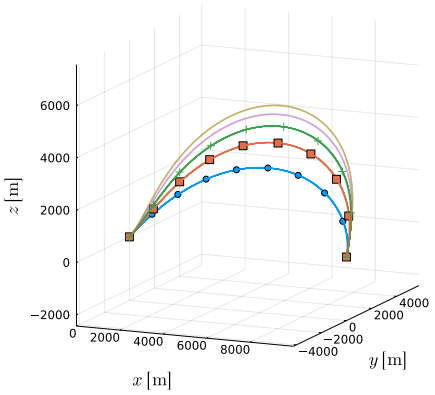

(a) Three-Dimensional Trajectory

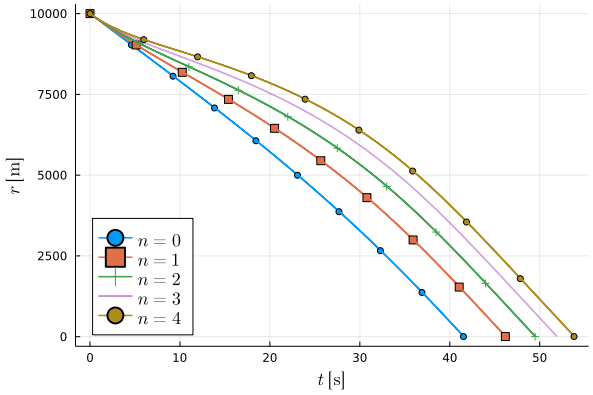

(b) Range

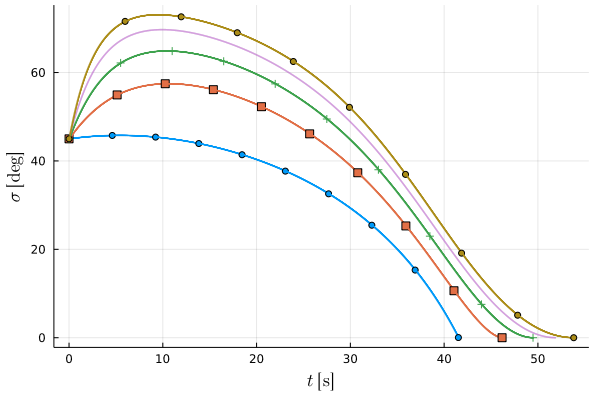

(c) Lead Angle

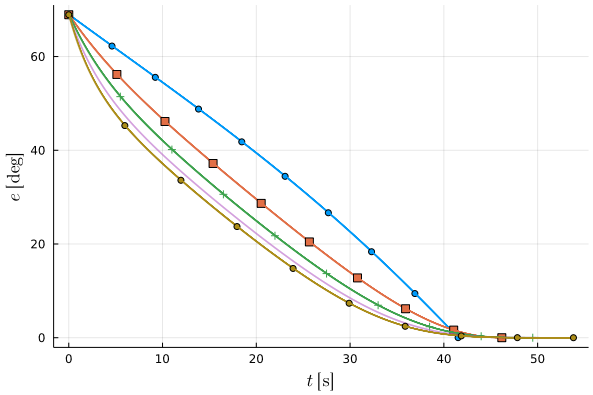

(d) Predicted Final Direction Error

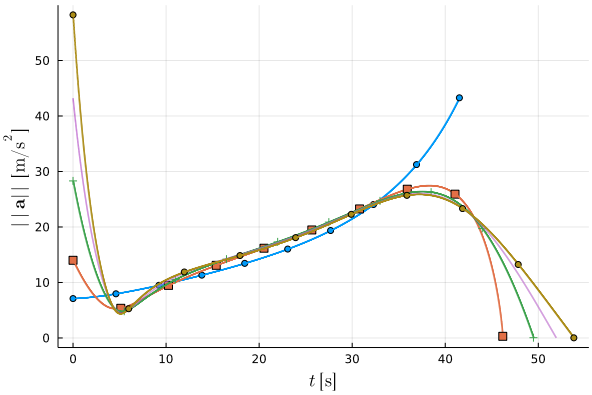

(e) Magnitude of Acceleration

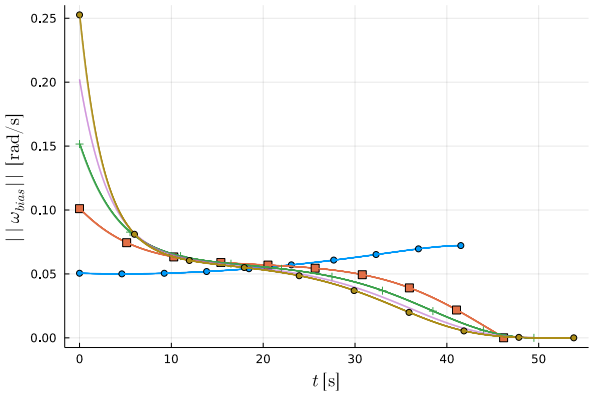

(f) Magnitude of Bias Angular Velocity Command

Fig. 7: Simulation Results for Case 2

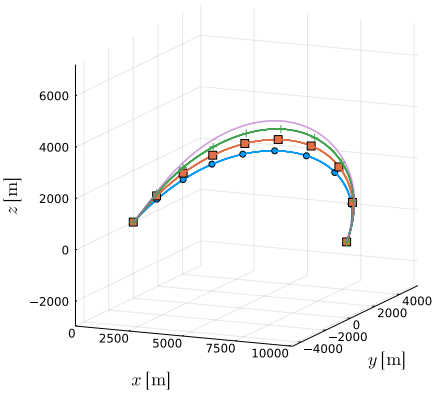

(a) Three-Dimensional Trajectory

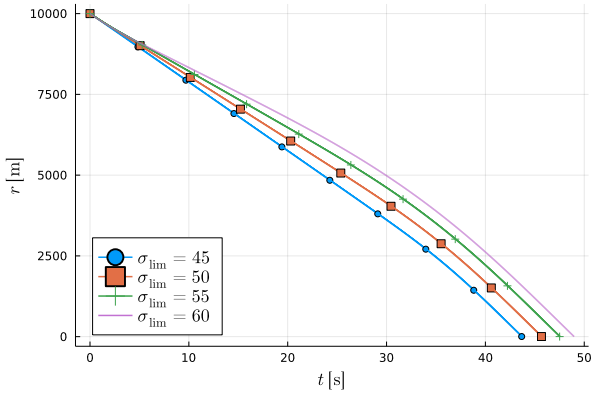

(b) Range

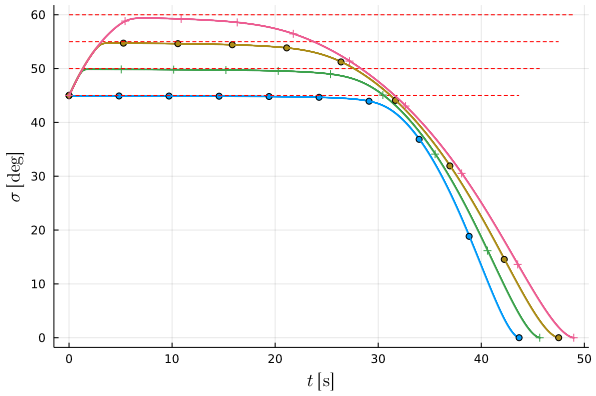

(c) Lead Angle

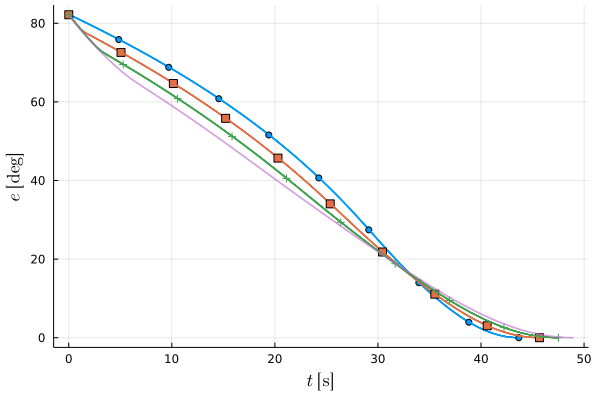

(d) Predicted Final Direction Error

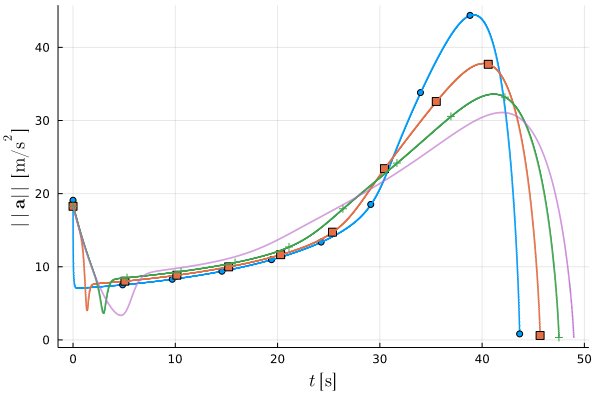

(e) Magnitude of Acceleration

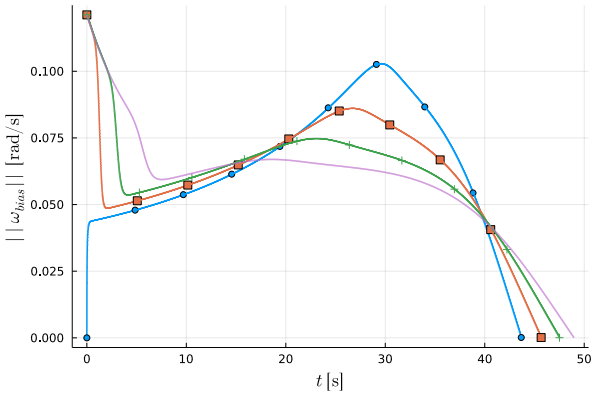

(f) Magnitude of Bias Angular Velocity Command

Fig. 8: Simulation Results for Case 3

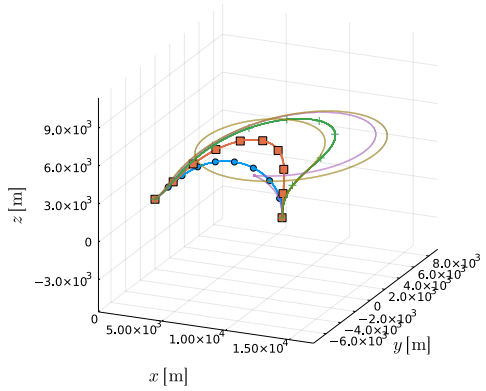

(a) Three-Dimensional Trajectory

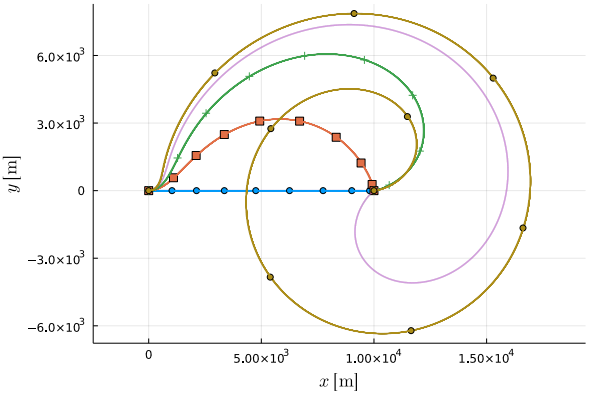

(b) Two-Dimensional Trajectory

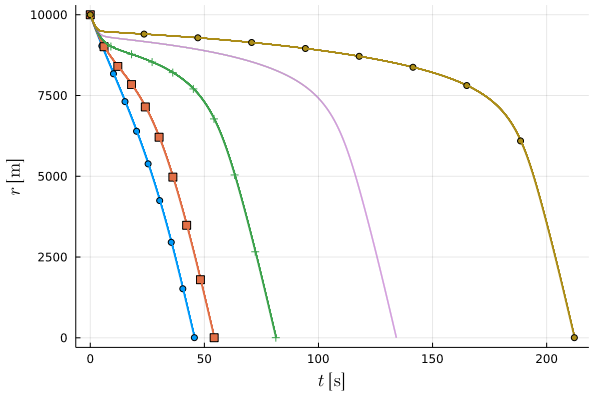

(c) Range

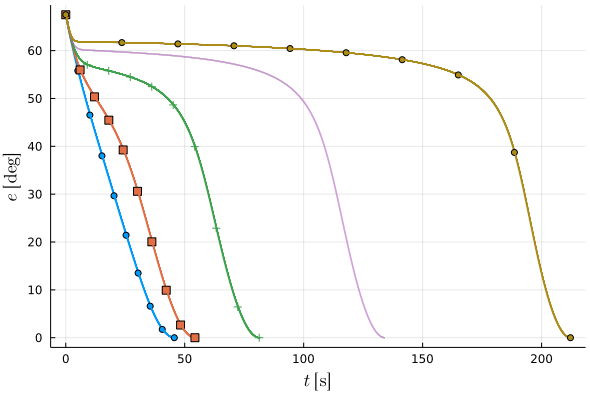

(d) Predicted Final Direction Error

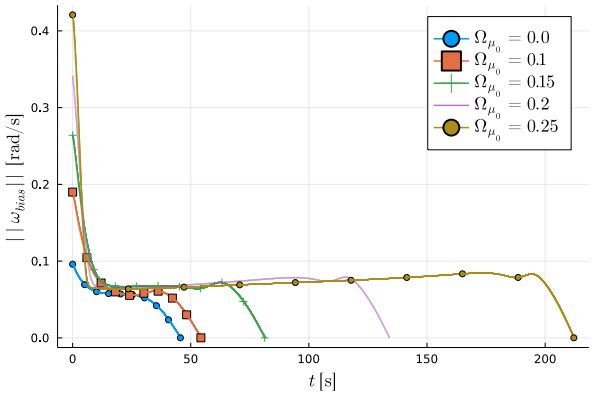

(e) Magnitude of Bias Angular Velocity Command

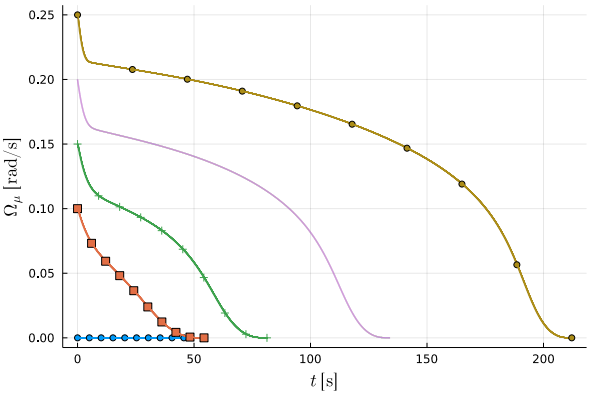

(f) Roll-like Angular Rate of Predicted Final Velocity

Fig. 9: Simulation Results for Case 4 – Evasive Manoeuvre

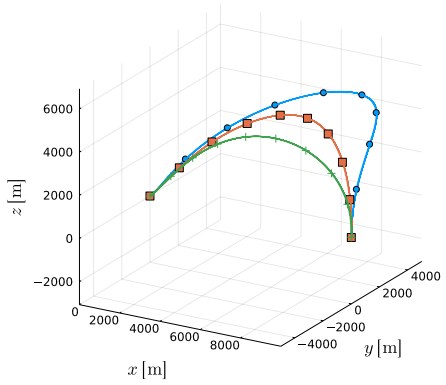

(a) Three-Dimensional Trajectory

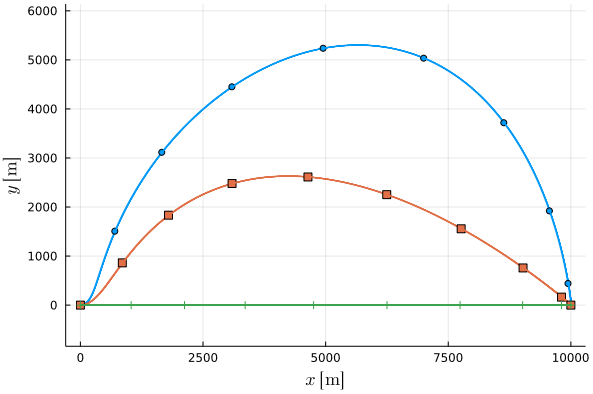

(b) Two-Dimensional Trajectory

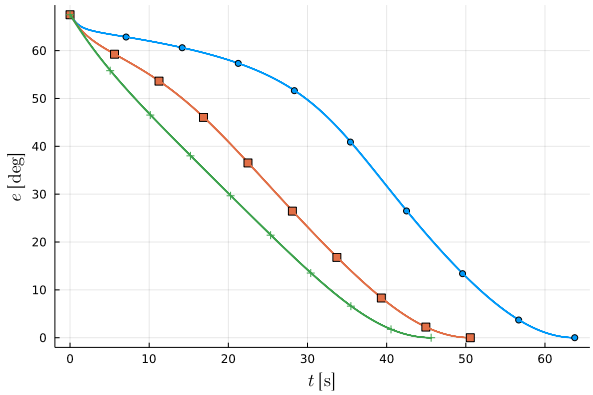

(c) Predicted Final Direction Error

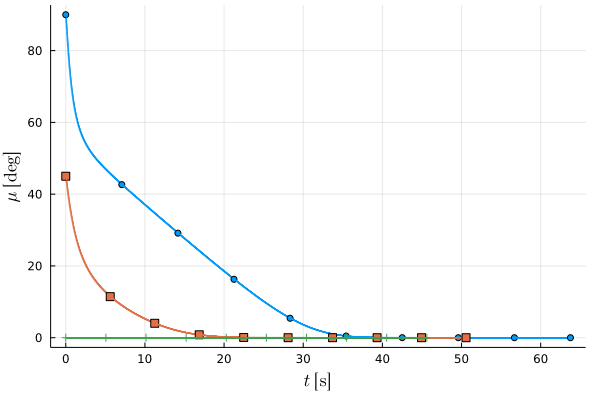

(d) Manoeuvre Plane Alignment Error

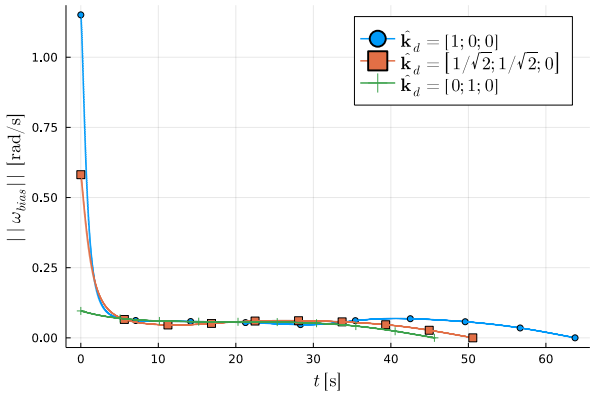

(e) Magnitude of Bias Angular Velocity Command

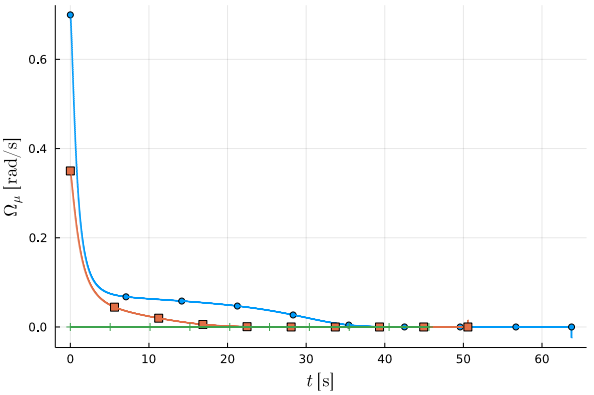

(f) Roll-like Angular Rate of Predicted Final Velocity

Fig. 10: Simulation Results for Case 4 – Desired Orientation of Manoeuvre Plane

Appendix

Modification Considering Look Angle Limit

An important aspect is to consider the constraint imposed on the look angle due to the limited field-of-view of forward-looking sensor, e.g., strapdown seeker in missiles. Assuming that the body-referenced look angle equals the velocity-referenced lead angle σ, one of the simplest ways to maintain σ within permissible range in the stationary target case is to deactivate the bias command as σ approaches the maximum allowable value σ_{lim}. This way of design modification is reasonable because the PPNG with a positive navigation ratio reduces the lead angle as it can be concluded from substituting Eq. (12) in Eq. (23). The concept of bias deactivation can be realised with multiplication of the bias angular velocity command an activation function $f_{\text{act}}(\sigma)$ such that $f_{\text{act}}(0) = 1$ and $f_{\text{act}}(\sigma_{\text{lim}}) = 0$ so that the guidance law becomes

$$\boldsymbol{\omega}_v = N\boldsymbol{\omega}_r^{r\perp} + f_{\text{act}}(\sigma)\,\boldsymbol{\omega}_{bias} \tag{A.1}$$

This approach is similar in its essence to the method developed in previous studies on guidance under look angle constraint such as [51]. The modification is also useful to ensure $\dot{r}(t) \leq 0$ for $\forall t \in \left[t_0, t_f\right]$ by taking $\sigma_{\text{lim}} = 90\,\text{deg}$, provided that $\dot{r}(t_0) \leq 0$.

References

[1] V. Tchuiev and T. Shima, "Intercept Angle Guidance in an Obstacle-Rich Environment," *Journal of Guidance, Control, and Dynamics*, vol. 40, no. 6, pp. 1507–1518, 2017.

[2] J.-S. Ha, H.-L. Choi, and J.-H. Jeon, "Iterative Methods for Efficient Sampling-Based Optimal Motion Planning of Nonlinear Systems," *International Journal of Applied Mathematics and Computer Science*, vol. 28, no. 1, pp. 155–168, 2018.

[3] M. A. Masoumnia, M. B. Menhaj, and A. Sooratgar, "A Unified Structure for Basic Guidance Laws of Moving Objects," *International Journal of Systems Science*, pp. 1–13, 2021.

[4] E. Bakolas, "Feedback Guidance in Uncertain Spatiotemporal Wind Using a Vector Backstepping Algorithm," *Journal of Guidance, Control, and Dynamics*, vol. 38, no. 4, pp. 631–642, 2015.

[5] D.-C. Liaw, C.-C. Cheng, and Y.-W. Liang, "Three-Dimensional Guidance Law for Landing on a Celestial Object," *Journal of Guidance, Control, and Dynamics*, vol. 23, no. 5, pp. 890–892, 2000.

[6] P. Lu, "Augmented Apollo Powered Descent Guidance," *Journal of Guidance, Control, and Dynamics*, vol. 42, no. 3, pp. 447–457, 2019.

[7] ——, "Theory of Fractional-Polynomial Powered Descent Guidance," *Journal of Guidance, Control, and Dynamics*, vol. 43, no. 3, pp. 398–409, 2020.

[8] M. Guelman, M. Idan, and O. M. Golan, "Three-Dimensional Minimum Energy Guidance," *IEEE Transactions on Aerospace and Electronic Systems*, vol. 31, no. 2, pp. 835–841, 1995.

[9] Y.-C. Chiou and C.-Y. Kuo, "Geometric Approach to Three-Dimensional Missile Guidance Problem," *Journal of Guidance, Control, and Dynamics*, vol. 21, no. 2, pp. 335–341, 1998.

[10] C.-Y. Kuo, D. Soetanto, and Y.-C. Chiou, "Geometric Analysis of Flight Control Command for Tactical Missile Guidance," *IEEE Transactions on Control Systems Technology*, vol. 9, no. 2, pp. 234–243, 2001.

[11] C. Li, W. Jing, H. Wang, and Z. Qi, "Gain-Varying Guidance Algorithm using Differential Geometric Guidance Command," *IEEE Transactions on Aerospace and Electronic Systems*, vol. 46, no. 2, pp. 725–736, 2010.

[12] R. W. Morgan, H. Tharp, and T. L. Vincent, "Minimum Energy Guidance for Aerodynamically Controlled Missiles," *IEEE Transactions on Automatic Control*, vol. 56, no. 9, pp. 2026–2037, 2011.

[13] G. Weiss and I. Rusnak, "All-Aspect Three-Dimensional Guidance Law Based on Feedback Linearization," *Journal of Guidance, Control, and Dynamics*, vol. 38, no. 12, pp. 2421–2428, 2015.

[14] N. Cho and Y. Kim, "Optimality of Augmented Ideal Proportional Navigation for Maneuvering Target Interception," *IEEE Transactions on Aerospace and Electronic Systems*, vol. 52, no. 2, pp. 948–954, 2016.

[15] H.-S. Shin, A. Tsourdos, and K.-B. Li, "A New Three-Dimensional Sliding Mode Guidance Law Variation With Finite Time Convergence," *IEEE Transactions on Aerospace and Electronic Systems*, vol. 53, no. 5, pp. 2221–2232, 2017.

[16] K.-B. Li, H.-S. Shin, A. Tsourdos, and M.-J. Tahk, "Performance of 3-D PPN Against Arbitrarily Maneuvering Target for Homing Phase," *IEEE Transactions on Aerospace and Electronic Systems*, vol. 56, no. 5, pp. 3878–3891, 2020.

[17] H.-S. Shin and K.-B. Li, "An Improvement in Three-Dimensional Pure Proportional Navigation Guidance," *IEEE Transactions on Aerospace and Electronic Systems*, pp. 1–1, 2021.

[18] Y.-H. Kim, C.-K. Ryoo, and M.-J. Tahk, "Guidance Synthesis for Evasive Maneuver of Anti-Ship Missiles Against Close-In Weapon Systems," *IEEE Transactions on Aerospace and Electronic Systems*, vol. 46, no. 3, 2010.

[19] N. Indig, J. Z. Ben-Asher, and N. Farber, "Near-Optimal Spatial Midcourse Guidance Law with an Angular Constraint," *Journal of Guidance, Control, and Dynamics*, vol. 37, no. 1, pp. 214–223, 2014.

[20] K. S. Erer, "Biased Proportional Navigation Guidance for Impact Angle Control with Extension to Three-Dimensional Engagements," Ph.D. dissertation, Department of Mechanical Engineering, Middle East Technical University, Ankara, Turkey, 2015.

[21] K. S. Erer and R. Tekin, "Impact Vector Guidance," *Journal of Guidance, Control, and Dynamics*, vol. 44, no. 10, pp. 1892–1901, 2021.

[22] J.-H. Kim, S.-S. Park, K.-K. Park, and C.-K. Ryoo, "Quaternion Based Three-Dimensional Impact Angle Control Guidance Law," *IEEE Transactions on Aerospace and Electronic Systems*, vol. 57, no. 4, pp. 2311–2323, 2021.

[23] K. S. Erer, R. Tekin, and M. K. Özgören, "Composite Impact Vector Control Based on Apollo Descent Guidance," *Chinese Journal of Aeronautics*, 2021.

[24] H. Li, J. Wang, S. He, and C.-H. Lee, "Nonlinear Optimal 3-D Impact-Angle-Control Guidance against Maneuvering Targets," *IEEE Transactions on Aerospace and Electronic Systems*, vol. 58, no. 3, pp. 2467–2481, 2022.

[25] S. Park, "Autonomous Aerobatics on Commanded Path," *Aerospace Science and Technology*, vol. 22, no. 1, pp. 64–74, 2012.

[26] N. Cho, Y. Kim, and S. Park, "Three-Dimensional Nonlinear Differential Geometric Path-Following Guidance Law," *Journal of Guidance, Control, and Dynamics*, vol. 38, no. 12, pp. 2366–2385, 2015.

[27] R. Tekin and K. S. Erer, "Three-Dimensional Formation Guidance with Rigidly Connected Virtual Leaders," *Journal of Guidance, Control, and Dynamics*, vol. 44, no. 6, pp. 1229–1236, 2021.

[28] D. Serakos and C.-F. Lin, "Three-Dimensional Mid-Course Guidance State Equations," *American Control Conference*, San Diego, CA, USA, June 1999.

[29] Y. Ulybyshev, "Terminal Guidance Law Based on Proportional Navigation," *Journal of Guidance, Control, and Dynamics*, vol. 28, no. 4, pp. 821–824, 2005.

[30] P. Lu, D. B. Doman, and J. D. Schierman, "Adaptive Terminal Guidance for Hypervelocity Impact in Specified Direction," *Journal of Guidance, Control, and Dynamics*, vol. 29, no. 2, pp. 269–278, 2006.

[31] H. B. Oza and R. Padhi, "Impact-Angle-Constrained Suboptimal Model Predictive Static Programming Guidance of Air-to-Ground Missiles," *Journal of Guidance, Control, and Dynamics*, vol. 35, no. 1, pp. 153–164, 2012.

[32] X. Wang and J. Wang, "Partial Integrated Guidance and Control for Missiles with Three-Dimensional Impact Angle Constraints," *Journal of Guidance, Control, and Dynamics*, vol. 37, no. 2, pp. 644–657, 2014.

[33] A. Maity, H. B. Oza, and R. Padhi, "Generalized Model Predictive Static Programming and Angle-Constrained Guidance of Air-to-Ground Missiles," *Journal of Guidance, Control, and Dynamics*, vol. 37, no. 6, pp. 1897–1913, 2014.

[34] S. Ghosh, D. Ghose, and S. Raha, "Composite Guidance for Impact Angle Control Against Higher Speed Targets," *Journal of Guidance, Control, and Dynamics*, vol. 39, no. 1, pp. 98–117, 2016.

[35] S. Ghosh, O. A. Yakimenko, D. T. Davis, and T. H. Chung, "Unmanned Aerial Vehicle Guidance for an All-Aspect Approach to a Stationary Point," *Journal of Guidance, Control, and Dynamics*, vol. 40, no. 11, pp. 2871–2888, 2017.

[36] B. Biswas, A. Maity, and S. R. Kumar, "Finite-Time Convergent Three-Dimensional Nonlinear Intercept Angle Guidance," *Journal of Guidance, Control, and Dynamics*, vol. 43, no. 1, pp. 146–153, 2020.

[37] R. V. Nanavati, S. R. Kumar, and A. Maity, "Spatial Nonlinear Guidance Strategies for Target Interception at Pre-Specified Orientation," *Aerospace Science and Technology*, vol. 114, p. 106735, 2021.

[38] ——, "Lead-Angle-Based Three-Dimensional Guidance for Angle-Constrained Interception," *Journal of Guidance, Control, and Dynamics*, vol. 44, no. 1, pp. 190–199, 2021.

[39] C. F. Lin and L. L. Tsai, "Analytical Solution of Optimal Trajectory-Shaping Guidance," *Journal of Guidance, Control, and Dynamics*, vol. 10, no. 1, pp. 60–66, 1987.

[40] M. N. Rao, "Analytical Solution of Optimal Trajectory-Shaping Guidance," *Journal of Guidance, Control, and Dynamics*, vol. 12, no. 4, pp. 600–601, 1989.

[41] E. J. Ohlmeyer and C. A. Phillips, "Generalized Vector Explicit Guidance," *Journal of Guidance, Control, and Dynamics*, vol. 29, no. 2, pp. 261–268, 2006.

[42] G. A. Harrison, "Hybrid Guidance Law for Approach Angle and Time-of-Arrival Control," *Journal of Guidance, Control, and Dynamics*, vol. 35, no. 4, pp. 1104–1114, 2012.

[43] C.-H. Lee, T.-H. Kim, and M.-J. Tahk, "Interception Angle Control Guidance Using Proportional Navigation with Error Feedback," *Journal of Guidance, Control, and Dynamics*, vol. 36, no. 5, pp. 1556–1561, 2013.

[44] C.-H. Lee and M.-G. Seo, "New Insights into Guidance Laws with Terminal Angle Constraints," *Journal of Guidance, Control, and Dynamics*, vol. 41, no. 8, pp. 1832–1837, 2018.

[45] S. He and C.-H. Lee, "Optimality of Error Dynamics in Missile Guidance Problems," *Journal of Guidance, Control, and Dynamics*, vol. 41, no. 7, pp. 1624–1633, 2018.

[46] N. Cho, "FlightGNC.jl," October 2021. [Online]. Available: https://github.com/nhcho91/FlightGNC.jl

[47] J. S. W. Wong, "On Vector Representation of Rigid Body Rotation," *Mathematics Magazine*, vol. 41, no. 1, pp. 28–29, 1968.

[48] H. W. Hickey, "More on Vector Representation of Rigid Body Rotation," *Mathematics Magazine*, vol. 43, no. 1, pp. 38–39, 1970.

[49] J. S. Dai, "Euler–Rodrigues formula variations, quaternion conjugation and intrinsic connections," *Mechanism and Machine Theory*, vol. 92, pp. 144–152, 2015.

[50] N. Cho, Y. Kim, and H.-S. Shin, "Generalized Formulation of Linear Nonquadratic Weighted Optimal Error Shaping Guidance Laws," *Journal of Guidance, Control, and Dynamics*, vol. 43, no. 6, pp. 1143–1153, 2020.

[51] N. Cho and S. Lee, "Look-Angle-Constrained Control of Arrival Time with Exact Knowledge of Time-to-Go," *Journal of Guidance, Control, and Dynamics*, vol. 44, no. 10, pp. 1902–1908, 2021.